Journal of Structural Geology 55 (2013) 1–20

Contents lists available at ScienceDirect

Journal of Structural Geology

journal homepage: www.elsevier.com/locate/jsg

Growth of normal faults in multilayer sequences: A 3D seismic case study from the Egersund Basin, Norwegian North Sea

Anette B.M. Tvedt [a,b,*], Atle Rotevatn [a,b], Christopher A.-L. Jackson [c], Haakon Fossen [a,b], Robert L. Gawthorpe [b]

[a] Centre for Integrated Petroleum Research, University of Bergen, Allégaten 41, 5007 Bergen, Norway
[b] Department of Earth Science, University of Bergen, Allégaten 41, 5007 Bergen, Norway
[c] Department of Earth Science & Engineering, Imperial College, London SW7 2BP, UK

ARTICLE INFO

Article history:
Received 2 November 2012
Received in revised form
29 July 2013
Accepted 7 August 2013
Available online 14 August 2013

Keywords:
Salt tectonics
Fault reactivation
Throw-length distribution
Expansion index
Fault linkage
Vertical throw-distribution

ABSTRACT

We investigate the structural style and evolution of a salt-influenced, extensional fault array in the Egersund Basin (Norwegian North Sea) through analysis of 3D reflection seismic and well data. Analysis of fault geometry/morphology, throw distribution and syn-kinematic strata reveal an intricate but systematic style of displacement and growth, suggesting an evolution of (1) initial syn-sedimentary fault growth contemporaneous with salt mobilization initiated during the Late Triassic, (2) cessation of fault activity and burial of the stagnant fault tips, and (3) subsequent nucleation of new faults in the cover above contemporaneous salt re-mobilization initiated during the Late Cretaceous, with downward propagation and linkage with faults. Stage 3 was apparently largely controlled by salt mobilization in response to basin inversion, as reactivated faults are located where the underlying salt is thick, while the non-reactivated faults are found where salt is depleted. Based on the 3D-throw analyses, we conclude that a combination of basement faulting and salt (re-) mobilization is the driving mechanisms behind fault activation and reactivation. Even though the sub- and supra-salt faults are mainly geometrically decoupled through the salt, a kinematic coupling must have existed as sub-salt faults still affected nucleation and localization of the cover faults.

1. Introduction

The structural style and evolution of normal fault arrays developing in the presence of mechanically weak detachments rich in, for example, halite (salt) or mudstone, are different to and less well understood than, fault arrays forming in the absence of such detachments. These differences arise in part due to the ability of salt and mudstone to accommodate strain and displacement by ductile flow. For example, salt- or mudstone-rich layers can: (i) act as regional detachment horizon or *décollement* (Morley et al., 2003; Jackson and Hudec, 2005); (ii) inhibit the vertical or lateral propagation of faults (e.g. Withjack et al., 1990; Pascoe et al., 1999; Maurin and Niviere, 2000; Withjack and Callaway, 2000; Richardson et al., 2005; Ford et al., 2007; Kane et al., 2010; Marsh et al., 2010); and (iii) cause full or partial geometric and kinematic decoupling of sub- and supra-detachment deformation (e.g. Stewart et al., 1997; Withjack and Callaway, 2000; Ford et al., 2007). Hence, ductile layers may significantly affect the geometry and evolution of extensional fault arrays, resulting in marked temporal and spatial variations in structural style, fault-related folding and displacement distribution (e.g. Rowan et al., 1999; Kane et al., 2010; Marsh et al., 2010; Duffy et al., 2012). The impact of ductile layers on normal fault array evolution becomes even more complex when polyphase extension occurs, because a second phase of extension can lead to: (i) reactivation of sub-detachment, typically 'thick-skinned' faults, and triggering of 'thin-skinned' extension of the supra-detachment cover; and (ii) the growth of salt- and shale-cored structures due to thin-skinned extension of the cover, which can itself cause faulting of the overburden (e.g. 'reactive diapirism'; Vendeville and Jackson, 1992; Jackson and Vendeville, 1994; Van Rensbergen et al., 1999).

Relatively few studies have addressed the structural style and evolution of normal fault arrays forming in response to salt- or mudstone-influenced, polyphase extension (Richardson et al., 2005; Kane et al., 2010; Duffy et al., 2012). The aims of this study are to: (i) highlight the relative roles of sub-salt 'basement' reactivation and salt mobilization, on the distribution and magnitude

* Corresponding author. Uni CIPR, PO Box 7800, N-5020 Bergen, Norway. Tel.: +47 97562768, +47 55583650.
E-mail address: Anette.B.Tvedt@uni.no (A.B.M. Tvedt).

0191-8141/$ – see front matter © 2013 Elsevier Ltd. All rights reserved.
http://dx.doi.org/10.1016/j.jsg.2013.08.002

of supra-salt 'cover' deformation; (ii) assess the impact that salt has on the magnitude of kinematic coupling between supra- and sub-salt faulting; and (iii) determine how mudstone layers influence the growth of normal fault systems in the supra-detachment sequence. To achieve these aims we use high-quality, 3D seismic reflection data (PGS MC3D-EGB2005) from the Egersund Basin, offshore Norway (Figs. 1 and 2), which allow us to constrain, in three-dimensions, the spatial relationship between, geometry and distribution of displacement on basement and cover faults, and thickness changes in coeval growth strata. Borehole data allows us to directly constrain the composition of the faulted sequence, and provide insight into the growth rate and spatial evolution of the studied fault array. Our results provide new insight into the control of polyphase rifting and ductile layers on the temporal and spatial evolution of normal fault arrays.

2. Geological framework

The Egersund Basin trends NW–SE and represents the NW extension of the Norwegian Danish Basin (Fig. 1). The basin initially formed in response to Carboniferous-to-Permian rifting (Sørensen et al., 1992; Ziegler, 1992). A thick succession of continental sediments was deposited in the basin during the Early Permian (Sørensen et al., 1992). During the Late Permian, the Egersund Basin represented a sub-basin of the 'North Permian Basin' (Sørensen et al., 1992; Ziegler, 1992), which formed following the syn- to

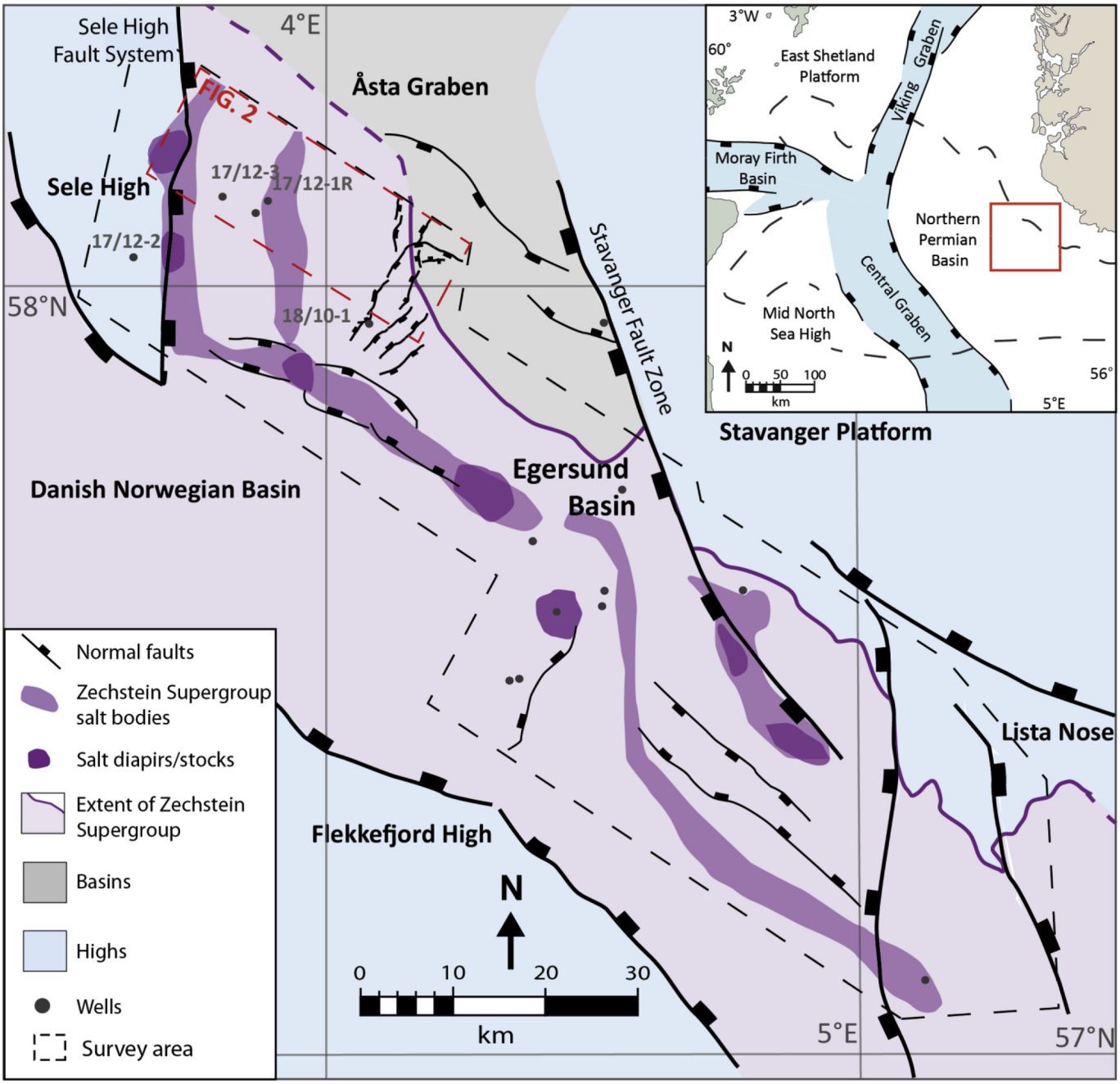

Fig. 1. Location of the Egersund Basin (EGB) in the North Sea north east of the Central Graben (red square in the inset of simplified structural map of the North Sea). Structural maps and extent of ZSG is based on observations in this study with data from Millennium Atlas (Zanella and Coward, 2003) and data from the Norwegian Petroleum Directorate. (For interpretation of the references to colour in this figure legend, the reader is referred to the web version of this article.)

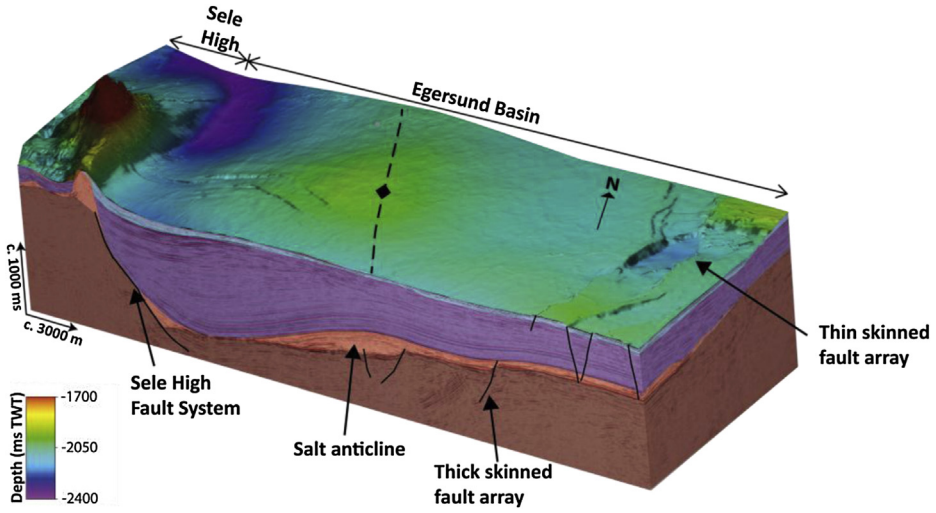

Fig. 2. Block diagram indicating the location of the studied fault array related to the salt anticline to the east. Horizon displayed on the top of the block is the top of the Bryne Formation. The colours on the sides of the block represent the age of the stratigraphy: Brown = Permian, Light red = Zechstein Supergroup, Purple = Triassic and Blue = Jurassic. (For interpretation of the references to colour in this figure legend, the reader is referred to the web version of this article.)

post-orogenic extensional collapse of the Variscan Orogen (Hodgson et al., 1992; Sørensen et al., 1992). Repeated flooding and desiccation of the North Permian Basin resulted in deposition of a thick (1000–1500 m; Sørensen et al., 1992) salt-rich succession (the Zechstein Supergroup; Hodgson et al., 1992; Sørensen et al., 1992; Davison et al., 2000; Glennie et al., 2003). Early Triassic rifting triggered flow and reactive rise of the salt, and formation of a variety of salt structures. The faults investigated in the study area nucleated in the supra-salt cover at this time (Sørensen et al., 1992).

Lower Jurassic deposits are absent in the Egersund Basin (Figs. 2 and 3) due to formation of the Mid-North Sea Dome during the Early Jurassic (Husmo et al., 2003). Subsequent rifting during the Middle Jurassic initiated in response to deflation of the dome (Underhill and Partington, 1993; Husmo et al., 2003), causing reactivation of major NW–SE-striking normal faults that bound the Egersund Basin (Sørensen et al., 1992). Syn-tectonic deposition of the Bryne, Sandnes, Egersund, Tau and Sauda Formations (Fig. 3) documents net-deepening of the basin during the Middle to Late Jurassic (Vollset and Doré, 1984). Extension rates decreased (Møller and Rasmussen, 2003), and a marine transgression occurred during the Early Cretaceous, resulting in deposition of deep-water mudstone and marl (Flekkefjord, Åsgård, Sola, and Rødby Formations) (Fig. 3) (Vollset and Doré, 1984; Isaksen and Tonstad, 1989). Rifting eventually ceased in the Late Early Cretaceous, and a period of basin shortening and inversion, probably related to the onset of the Alpine orogenic event, occurred during the Late Cretaceous, leading to folding, salt re-mobilisation and reverse reactivation of pre-existing, rift-related faults (Ziegler, 1992; Vejbæk and Andersen, 2002; Jackson and Lewis, 2012; Jackson et al., 2013).

3. Data and methodology

3.1. Database

The database for this study comprises a pre-stack time-migrated, three-dimensional reflection seismic survey (PGS MC3D-EGB2005), tied to 13 wells. The study area covers an area of 552 km^2 in the north-western part of the Egersund Basin (Figs. 1 and 2). Crossline and inline spacing are 25 m, and the seismic sections are displayed with reverse polarity, so that an increase in acoustic impedance is presented by a trough (red), while a decrease in acoustic impedance is represented by a peak (black) (SEG European Convention; Brown, 2003). Crosslines are orientated NE-SW and inlines are orientated NW–SE. The vertical seismic resolution in the interval of interest is c. 20–40 m, based on a frequency range of 25–35 Hz and velocity range of 2700–3700 ms^{-1}.

The age of the mapped seismic horizons and the lithology of the stratigraphic intervals they bound, were constrained by formation top data from 13 wells (Fig. 1; Table 1). We mapped 24 faults in the studied fault array, and 15 were subject to quantitative analysis of throw. Fourteen seismic horizons were mapped to constrain the throw distributions on the fault surfaces, and thickness variations in stratigraphy adjacent to the faults. Both fault throw and growth strata thickness patterns provide insights into the growth history of individual fault segments and the array as a whole.

3.2. Methodology

Four methods were used to determine the growth history of the studied fault array: (i) creation of throw-length (*T-x*) plots, which allow the map-view growth history of the faults to be assessed (Walsh and Watterson, 1990; Childs et al., 1995; Gawthorpe and Leeder, 2000); (ii) creation of throw-depth (*T-z*) plots, which provide insights into the potential role of dip linkage on fault growth (Mansfield and Cartwright, 1996; Hongxing and Anderson, 2007), and which allow us to discriminate between periods of syn-sedimentary faulting and blind fault propagation (e.g. Williams et al., 1989; Nicol et al., 1996); (iii) strike-projections of fault throw, which illustrate throw distribution across fault surfaces and provide insights into the growth and linkage history of segmented normal fault systems (Walsh and Watterson, 1991); and (iv) generation of time-thickness (isochron) maps and expansion indices for key stratigraphic intervals, which together illustrate variations in sediment thickness adjacent to and reveal the growth history of, fault systems and arrays (Thorsen, 1963; Rouby et al., 2003; Jackson and Rotevatn, 2013). The use of isochron maps to constrain the growth of normal faults is only valid if sedimentation rate exceeds or is comparable to fault displacement rates (Childs et al., 2003), which we will demonstrate is the case for the Egersund Basin.

Fault throw was constrained by measuring differences between the footwall and hanging wall horizon cut-offs on seismic profiles

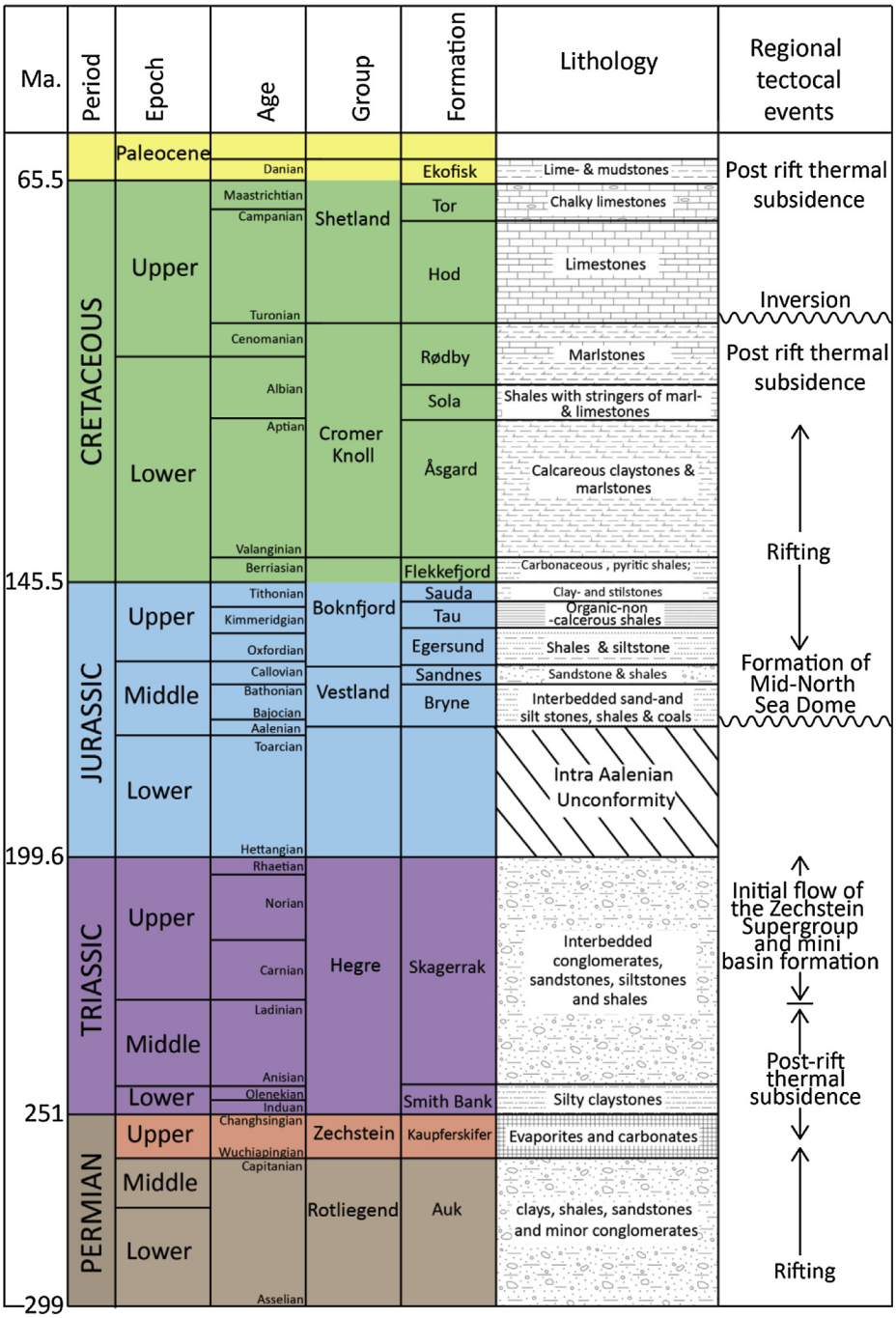

Fig. 3. Stratigraphic framework showing the key seismic horizons, their ages and information about the evolution of the Egersund Basin. Colour coding of the different periods is continued throughout the article. (For interpretation of the references to colour in this figure legend, the reader is referred to the web version of this article.)

(generally inlines) oriented perpendicular to local fault strike. Throw was recorded every 100–600 m, depending on the degree of structural complexity and rapidity of along-strike throw variations. The error of throw measurements in the Middle Jurassic and post-Aptian succession is small and estimated to ±4 ms, based on the generally excellent quality of the seismic data. However, data quality and resolution deteriorates in the Triassic succession as well as in the Tithonian to Aptian interval, where we estimated throw measurement errors to be ±6 ms. Where folds are developed adjacent to the fault surfaces, we record fault throw values that include and exclude the ductile component of deformation.

We use check-shot velocity data from nearby wells (18/10-1, 17/12-1 and 17/12-2; Table 1) to depth convert throw values recorded in time (ms TWT) to metres. This exercise indicates that the patterns and shapes of throw variations on *T-z* plots are the same in both the time and depth domains, so we elect to present all throw values in milliseconds two-way time (ms TWT) (Fig. 4). Well data and seismic facies observations suggest that limited lateral sedimentological heterogeneity exists in the faulted succession, which together with small throw values leads us to believe that the effects of differential compaction across the studied faults is negligible (Mansfield and Cartwright, 1996).

Table 1
Wells within the Egersund Basin (Data from the Norwegian Petroleum Directorate).

Well	TD depth (m RKB)	Oldest penetrated stratigraphic unit
17/12-1R	4298	Zechstein
17/12-2	2334	Devonian (no formation defined)
17/12-3	2730	Skagerrak
18/10-1	2800	Skagerrak
9/2-1	3755	Skagerrak
9/2-2	3548	Skagerrak
9/2-3	3421	Bryne
9/2-4s	3313	Bryne
9/2-5	3354	Bryne
9/2-6s	3642	Bryne
9/2-8s	3345	Zechstein
9/2-11	2836	Bryne
9/3-1	1970	Skagerrak
9/3-2	3151	Skagerrak

4. Description of the salt-influenced fault array

The fault array contains a wide range of normal fault geometries and styles of linkage. For descriptive purposes, the fault array is divided into a *basement-restricted fault array* (i.e. faults that tip-out upward into the salt), *cover-restricted fault array* (i.e. faults that tip-out downward into the salt) and a *basement-involved fault array* (i.e. faults that offset both sub- and supra-salt strata and the salt itself) (Fig. 5).

4.1. Geometry of the basement-restricted fault array

The basement-restricted fault array consists of faults which strike NNW-SSE and mainly dip to the west. A small subpopulation of faults, which are shorter and have less throw, are oriented at a large angle to this trend (Fig. 5a and b). The largest basement fault is 13.8 km long, has a maximum throw of 165 ms (314 m) at top basement level and is divided into four geometric segments. Throw on the basement-restricted faults typically varies between 80 and 140 ms (c. 150–266 m) (Fig. 6).

4.2. Geometry of the cover fault array

The NNE–SSW-trending, cover-restricted fault array is c. 16 km long, c. 6 km wide and consists of a series of WNW- or ESE-dipping, *en-echelon* normal fault segments that step progressively westward toward the north (Figs. 2 and 5c–f). The cover-restricted fault array occurs directly above the basement-related fault array, or along the southern part of the array it is laterally offset from it by up to 8 km. In the north–east of the array, mean fault strike changes from NNE–SSW to WNW–ESE (Fig. 5c–f). In cross-section, the majority of the cover-restricted faults are planar and dip 45–55° on the time-migrated seismic data. In map-view, the faults are straight or slightly curved. Based on the vertical extent (i.e. height) of their constituent fault segments, their location within the study area and their inferred style of growth, the cover-restricted fault array is divided into two geographic domains (northern and southern; Fig. 5d).

4.2.1. Northern Domain

Faults in the Northern Domain (Figs. 5d and 7) are 1 km to at least 3.2 km long, and they generally tip out downward either into a very thin (<30 ms or 55 m) salt layer or within the basement where salt is absent. The faults tip out upward within Triassic or Upper Jurassic strata (Fig. 7a and b). Many fault tips are overlain by low-relief (30 ms or 45 m) monoclines, especially above faults that do not breach the mudstone-rich Upper Jurassic interval (Fig. 7b). *T-z* plots (Fig. 7b) and throw strike-projections (Fig. 7d) for cover-restricted faults in the Northern Domain are typically characterized by an asymmetric throw distribution. For example, maximum throw (56 ms or 90 m) occurs at the centre of fault C1, near the top Triassic (Fig. 7b), gradually decreasing downward (throw gradient = 0.03) toward the lower Triassic, followed by an abrupt decrease in throw and marked increase in throw gradient (throw gradient = 0.30) from this stratigraphic level to the lower fault tip. Above the position of maximum throw, throw decreases relatively rapidly upward (throw gradient = 0.24) to just below the top of the Bryne Formation. Above this point, throw decreases at a lesser rate (throw gradient = 0.06) toward the upper fault tip, which occurs in the lower part of the Sauda Formation (Fig. 7b). Near the lateral tips of fault C1, where less throw occurs, the same gradual downward decrease in throw into the lower part of the Triassic succession is observed. In summary, *T-z* plots for cover-restricted faults in the northern domain contain three main inflection points and are thus characterized by: (i) high throw gradients just above where they terminate downward into the salt; (ii) gentle throw gradients within the Triassic succession; (iii) high throw gradients in the Middle Jurassic; and (iv) low throw gradients in the Lower Jurassic.

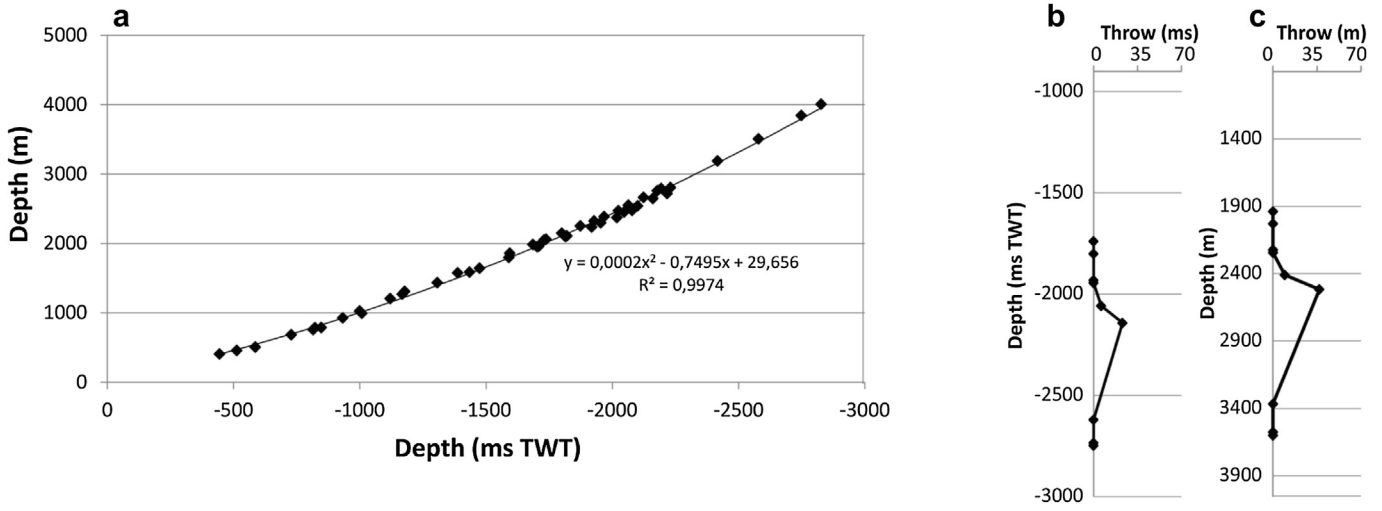

Fig. 4. (a) Graph for depth to travel-time comparison so as to determine the depth conversion formula, using check shots from three nearby wells; (b) Throw-time (ms) plot and (c) Throw – depth (m) differ in shape, but not geometry.

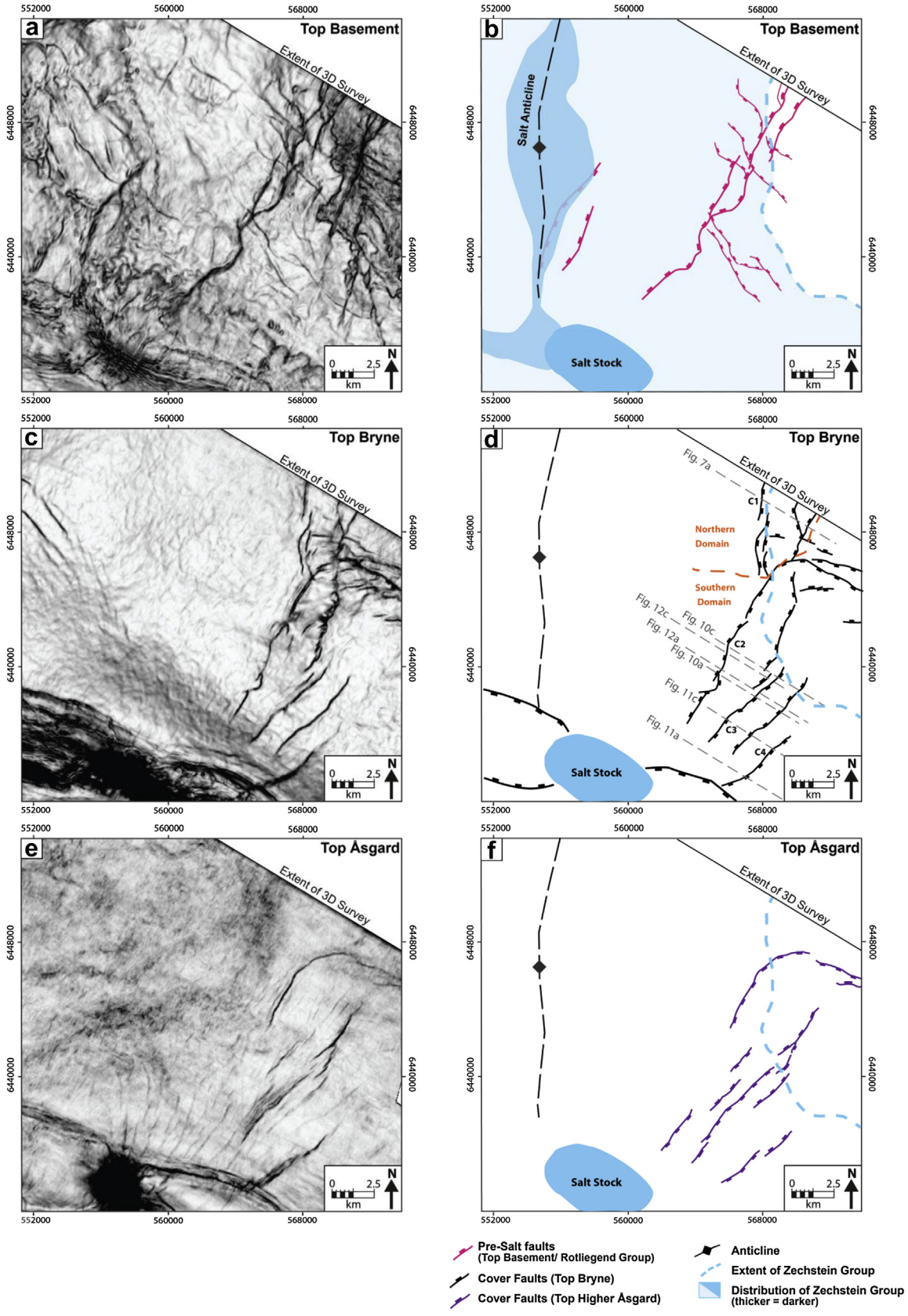

Fig. 5. Simplified maps of fault patterns based on fault interpretations and coherance discontinuities in the horizontal continuity of amplitude of the seismic (variance maps) for: (a) and (b) Basement (pre-Zechstein) fault array and salt distribution. (c) and (d) Cover faults at Middle Jurassic level for the Top Bryne Formation where the cover fault array has approximately its maximum throw. Figure lines for later figures included. (e) and (f) the cover fault array at a Middle Cretaceous level displayed on the Top Higher Åsgaard.

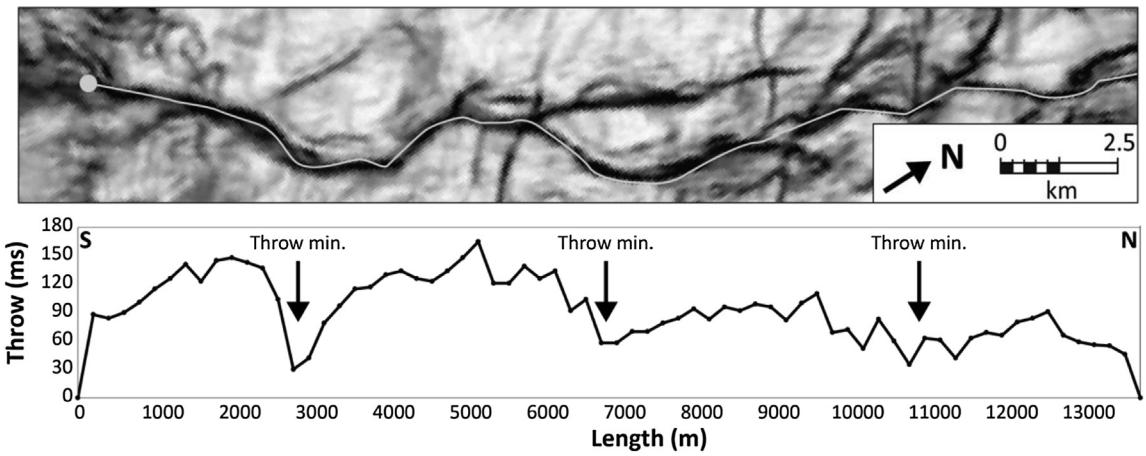

Fig. 6. Example variance map of a measured basement fault with corresponding D-L profile. The measured basement fault can be divided into at 4 hard linked segments based on the 3 throw minima.

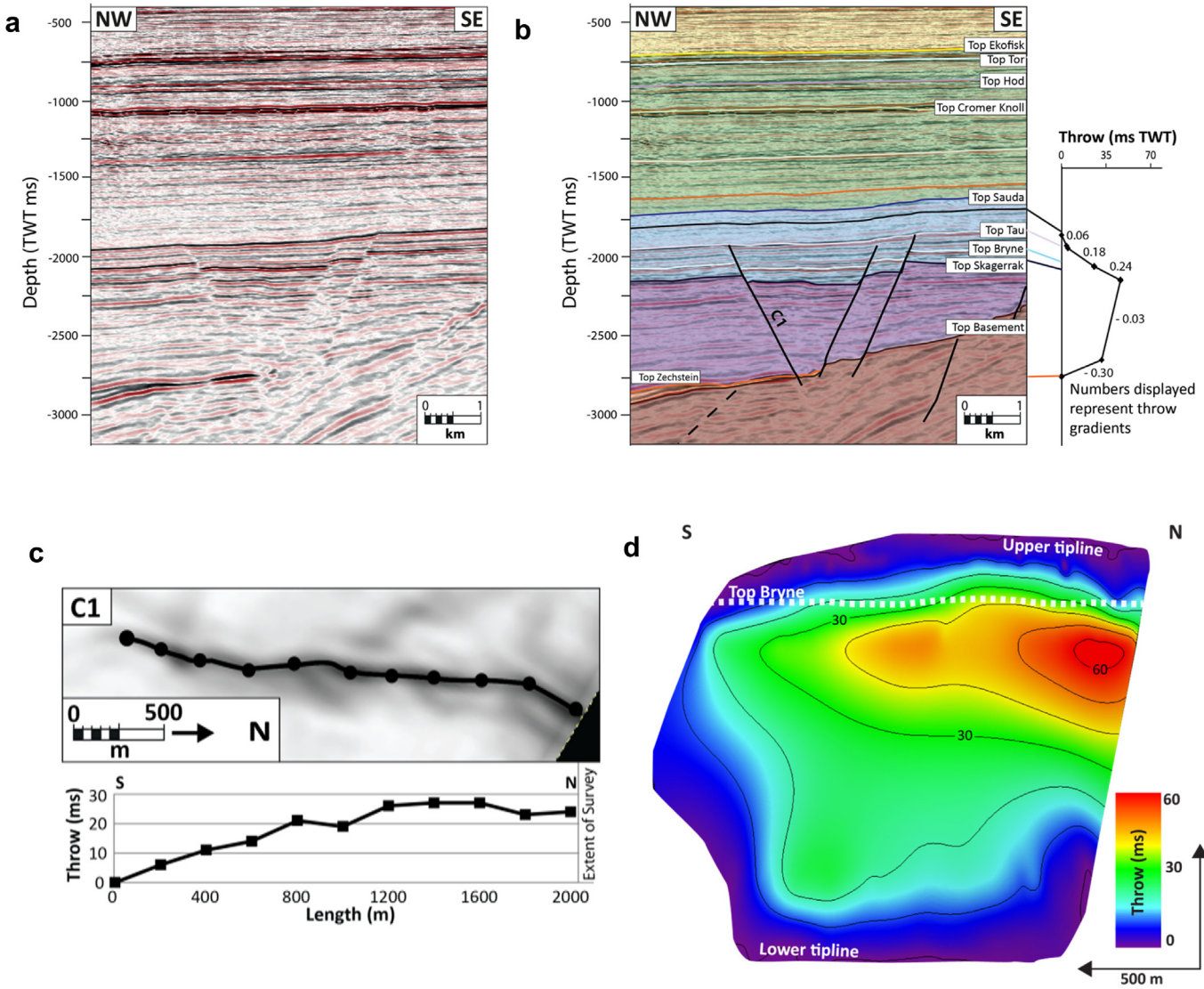

Fig. 7. (a) and (b) Seismic profile illustrating the cover fault C1 to the right, bound between the basement or very thin salt and Upper Jurassic strata. *T-z* plot shows an asymmetric, upward-truncated vertical-throw profile where the maximum throw is at the transition between Upper Triassic and Middle Jurassic. (c) Variance map of fault C1 in the Northern Domain with each selected point for the throw-length profile along the Top Bryne Formation. (d) Throw strike-projections with truncated contours toward the upper tipline.

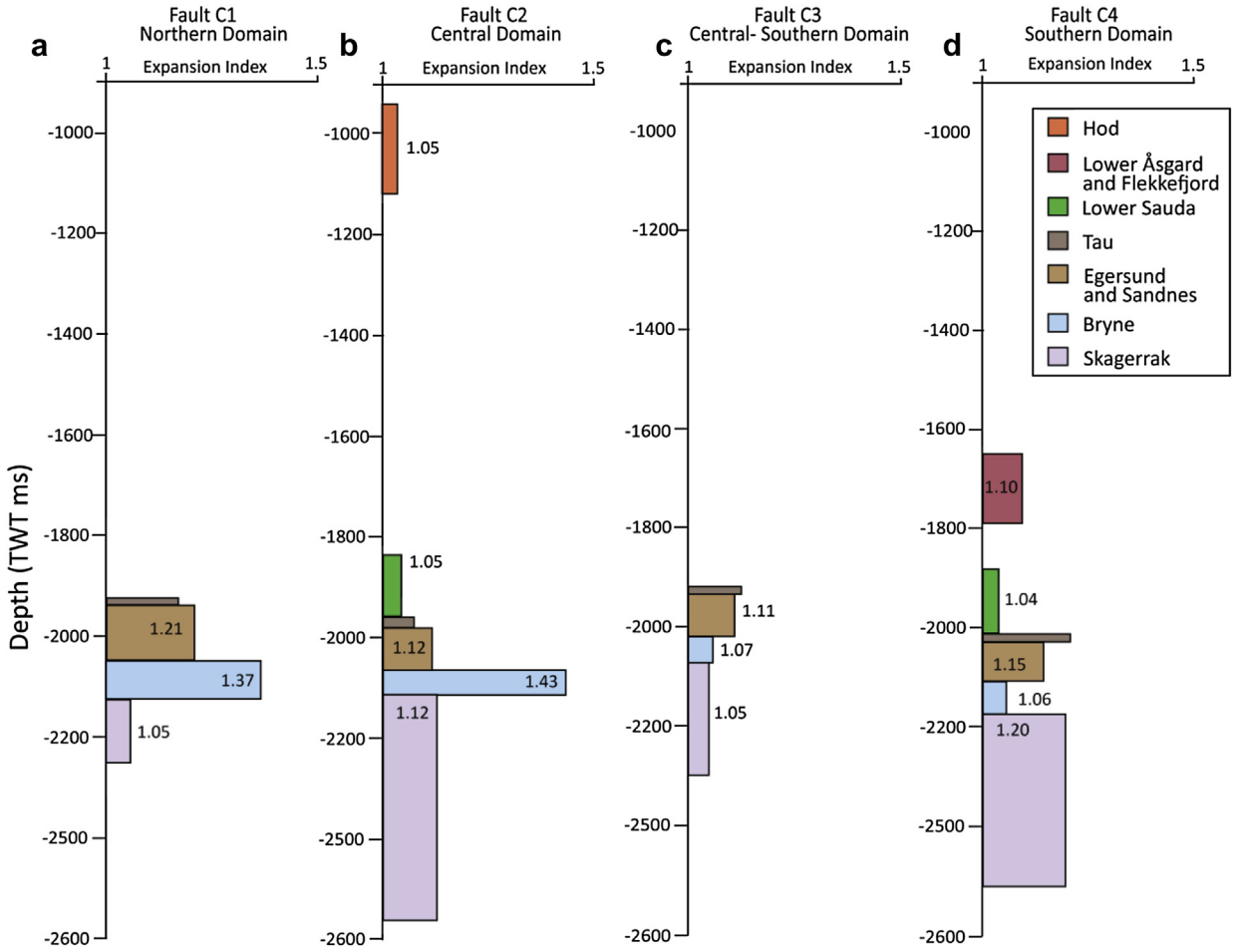

Fig. 8. Expansion indices showing growth in the hanging wall of faults; (a) C1 the Northern Domain with increasing fault growth from the deposition of the Skagerrak, Bryne, Sandnes, Egersund and Tau Formations. (b) C2 in the Southern Domain showing fault growth during deposition of the Skagerrak, Bryne, Egersund, Tau and Sauda Formations and during deposition of the Hod Formation. (c) C3 in the southern domain show fault growth during deposition of Skagerrak, Bryne, Egersund and Tau Formations. (d) C4 in the southern domain show fault growth during deposition of Skagerrak, Bryne, Egersund, Tau and the lower Åsgard and Flekkefjord Formations.

Expansion indexes indicate increased hanging wall thickness for the Skagerrak, Bryne Egersund Sandnes and Tau Formations (Figs. 8a and 9a–b).

4.2.2. Southern Domain

Faults in the Southern Domain strike NE-SW, dip NW or SE and are up to 6.2 km long (Fig. 5d). The majority of these faults tip out upward in Lower Cretaceous strata and downward into the salt.

T-z plots taken at the point of maximum throw, and strike-projections of throw on the fault surfaces indicates that, like the faults in the northern domain, faults in the Southern Domain are characterized by asymmetric throw distributions (Figs. 10–12). Several faults in the southernmost part of the Southern Domain bifurcate along strike, such that a single fault surface passes along-strike into two, laterally separate segments (e.g. C3 and C4; Figs. 1, 10 and 13a). Where two segments are developed, they are typically separated across and tip out into the mudstone-dominated Upper Jurassic interval. For example, seismic sections and *T-z* profiles (Fig. 10b) indicate that where throw on the structure is greatest (70 ms or 109 m), fault C3 consists of a single fault surface with throw distributed asymmetrically on the lower portion similar to northern domain faults, whereas the upper portion of the fault has more symmetrically distributed throw laterally and an overall c-shaped profile in the slip direction. Two throw maxima are observed on the fault: a lower one near the top of the Bryne Formation (70 ms and 109 m), and an upper one near the top of the Åsgard Formation (36 ms or 47 m) (Fig. 10b). Along strike to the north, C3 is represented by two discrete segments, with the upper and lower segments being stratigraphically restricted to the Lower Cretaceous and Triassic-to-Middle Jurassic intervals, respectively (Figs. 10d and 13a). In this location, mudstone-dominated strata of the Egersund, Tau and the Sauda Formations are undeformed, and maximum throw on the lower and upper segment occurs near the top of the Bryne (17 ms and 27 m) and Åsgard (16 ms or 21 m) Formations, respectively (Fig. 10d). A strike-projection of throw on fault C3 confirms that the upper and lower segments are only locally linked for about a 1 km long portion located near the centre of its 7.5 km length (Fig. 10f). Furthermore, Fig. 10f indicates that the lower segment has a strongly asymmetric throw distribution, whereas the upper segment is characterized by relatively symmetric, broadly elliptical throw contours. Expansion indices and isochron maps indicate increased hanging wall thickness for the Skagerrak, Bryne, Egersund and Tau Formations (Figs. 8c and 9a–c).

Fault C4 has the same general geometry as fault C3, and is a single fault where throw is greatest, and two physically separate segments laterally toward the fault tips (C4 in Fig. 5d; Fig. 11). However, *T-z* plots indicate that the point of maximum throw (127 ms or 227 m) on the lower segment is observed within the Triassic rather than near the top of the Middle Jurassic. Below this point, throw decreases gradually and gently downward

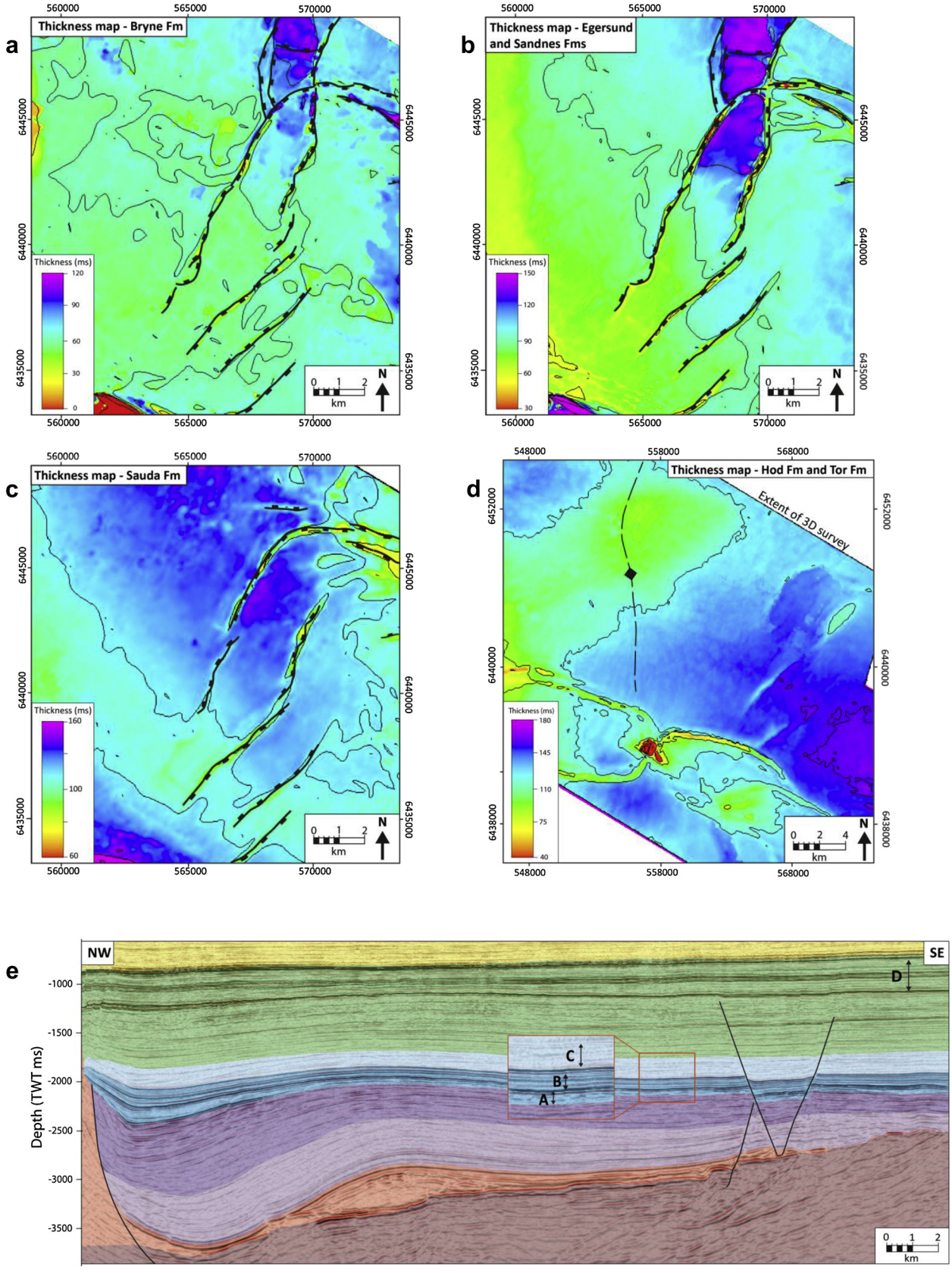

Fig. 9. Isochron thickness maps illustrating sediment thicknesses and depocentre migration of the: (a) Bryne Formation (Upper Triassic to Middle Jurassic) with increased hanging wall thickness in the graben toward the north, indicative of syn-sedimentary faulting during this time. (b) Sandnes and Egersund Formations (Middle -Upper Jurassic) where the depocentre migrated southward. (c) Lower part of Sauda Formation (Upper Jurassic) where the main depocentre migrated further south. (d) Tor and Hod Formations (Upper Cretaceous) with decreasing sediment thickness across the salt anticline (note the change of scale on this map). (e) Each interval used for time thickness maps is indicated by letters on figure showing thickness variations of sedimentary sequences. Upper Triassic and Middle Jurassic sediments (highlighted purple and blue colours) increase in thickness toward the NW indicating the initiation of the formation of a salt weld between the salt diapir and the salt anticline during this time. There is also a slight decrease in thickness from the east toward the top of the salt anticline of the Upper Triassic sediments which may indicate build-up of the salt anticline. Intra Aalenian unconformity is thought to have caused some of the thinning of the Skagerrak Formation across the salt anticline. (For interpretation of the references to colour in this figure legend, the reader is referred to the web version of this article.)

(throw gradient = 0.10) within the lower part of the Triassic, before abruptly and rapidly (throw gradient = 0.76) decreasing just above the salt. In this location, the top of the salt is offset by 100 ms (186 m), whereas the base of the salt (i.e. top basement) is not offset, even though the salt is relatively thin (<200 ms or 370 m) in this area (Fig. 11a–d and f). Above the point of maximum throw, throw decreases gradually upward toward the top of the Sauda Formation, thereby defining an overall asymmetric profile to the lower segment of C4. In contrast, the upper segment of fault C4 is characterized by a more symmetric distribution of throw and elongated, elliptical throw contours, which are centred on the point of maximum throw (32 ms or 42 m) in the upper part of the Åsgard Formation (Fig. 11f). Expansion indices and isochron thickness maps indicate increased hanging wall thickness for the Skagerrak, Bryne, Egersund, Tau and the lower Åsgard and Flekkefjord Formations (Figs. 8d and 9a–c).

The Tau and Egersund Formations are typically folded into low-relief (up to 50 ms or 75 m), 100–400 m wide synclines in the hangingwalls of faults in the Southern Domain (Figs. 10a–d, 11a–b and 12a–d). *T-z* profiles that include this ductile component of the deformation show that the large amount of folding occurs in the mudstone-dominated Upper Jurassic unit (Fig. 11b and d). The relief of the synclines increases with increasing fault throw (e.g. Tau Formation in Fig. 11b and d). Where the faults in the Southern Domain bifurcate along strike, these mudstone-dominated Upper Jurassic layers appear as low relief (22 ms or 33 m) monoclines above the upper tip-line of the lower segment of the fault (Fig. 10d).

4.3. Basement-involved faults

By definition, cover-restricted faults do not offset basement. However, cover fault C2, which is located in the western part of the Southern Domain, represents a notable exception because, along its northern portion, it is physically linked to a basement-involved fault (Figs. 12, and 13b). Where C2 is decoupled from the basement-involved fault, *T-z* profiles display an asymmetrical lower part located within Triassic-Upper Jurassic strata, and a slightly offset upper part within Upper Jurassic-Cretaceous strata (Fig. 12a–b). Two throw maxima are observed: a lower one at the top of the Skagerrak Formation (48 ms or 76 m) and an upper one at the top of the Åsgård Formation (10 ms or 14 m). Along strike to the north, where the cover-restricted and basement-restricted faults are physically linked and form a through-going fault, *T-z* profiles can be divided into three segments, where a lower asymmetric portion has throw maximum at top Basement (125 ms or 237 m) (Fig. 12c–d) with a rapid upward decreasing throw gradient (0.79) into the salt, an asymmetric middle portion and a symmetric upper part, which are similar to those observed along strike to the south. Strike-projections of throw display tightly spaced contours toward the lower fault tip. Tightly spaced contours are also observed toward the top of the Bryne Formation (Fig. 12f), whereas the uppermost portion of the fault displays more elliptical contours that are centred on maximum throw at the top of the Åsgård Formation. Expansion indices and isochron thickness maps indicates increased hanging wall thickness for the Skagerrak, Bryne, Egersund, Tau, Sauda and Hod Formations (Figs. 8b and 9a–d).

5. Growth of the thin-skinned fault array

Based on their stratigraphic occurrence (i.e. cover- or basement-restricted, or basement-involved) and growth histories, we define three type of faults: 1) cover-restricted growth faults formed by radial propagation of a single fault surface, 2) cover-restricted growth faults formed in response to dip-linkage of segments and 3) dip-segmented, basement-involved faults formed in response to upward propagation of a sub-salt fault into the cover.

5.1. Cover-restricted growth faults formed by radial propagation

Cover-restricted growth faults are mainly developed in the Northern Domain (Fig. 5d). Maximum throw is observed at the top of the Triassic succession, suggesting that the fault nucleated at this structural level. This interpretation is supported by the observation that Middle Jurassic strata thicken abruptly across these faults (Figs. 8 and 9a), which we also infer to mean that the faults nucleated in the very shallow subsurface and/or rapidly propagated upward to the free surface (Baudon and Cartwright, 2008a; Jackson and Rotevatn, 2013). Furthermore, high throw gradients near the upper tips of these faults are characteristic of syn-sedimentary growth faults (Fig. 14) (e.g. Nicol et al., 1996; Baudon and Cartwright, 2008a). The elliptical throw contours, which are centred on the position of maximum throw, and D-L profiles strongly suggest that the fault grew via radial propagation of its tips rather than via segment linkage (e.g. Watterson, 1986; Walsh and Watterson, 1988; Baudon and Cartwright, 2008a). The absence of Lower Jurassic strata make it is difficult to determine whether faulting also occurred during the Early Jurassic. Irrespective of the Early Jurassic history of these faults, the observation that the latest Middle Jurassic and Upper Jurassic succession (Sandnes, Egersund and Tau Formations) thicken across the faults, and that the upper tips are associated with high throw gradients, indicate that these faults were active in the Late Jurassic (Early Tithonian) (Figs. 7, 8a and 9a–b).

5.2. Cover-restricted growth faults formed by dip linkage of blind faults

Most faults in the Southern Domain of the cover fault array are longer and taller than faults in the Northern Domain, implying that they accommodated strain over a greater rock volume than their northern counterparts. Faults in the Southern Domain (Fig. 5d) are characterized by either a single, continuous fault surface that offset Triassic, Jurassic and Cretaceous strata (Figs. 10–12), or a fault surface that bifurcates along strike (Figs. 1, 10 and 13a). This variability in structural style, in combination with their more complex throws distributions, suggests that faults in the Southern Domain have a more complex growth history than those in the north. The asymmetric throw distribution of the lower fault segments of cover faults C2 and C3 show rapid upward decrease in throw from the point of maximum throw. Based on this observation, and expansion indices (Fig. 8b and c) and isochron maps (Fig. 9), we interpret that faults exemplified by C2 and C3 were syn-sedimentary growth faults that were active from the Triassic to Late Jurassic. Fault C4 has a slightly different throw profile, characterized by a gradual upward decrease from the point of maximum throw, which is indicative of a fault that propagated blind and did not breach the free surface. However, expansion indices (Fig. 8d) indicate that the fault breached the surface during the middle Triassic, and remained as surface-breaching structure until it was finally buried in the Kimmeridgian. The low throw gradients in the Triassic could possibly be explained by high sedimentation rates in the south.

C2, C3 and C4 all show elliptical throw contours centred on a second throw maximum located on the upper part of the fault. We suggest that this throw distribution results from a second phase of fault growth related to post-burial reactivation in the Southern Domain, which occurred by either 1) upward,

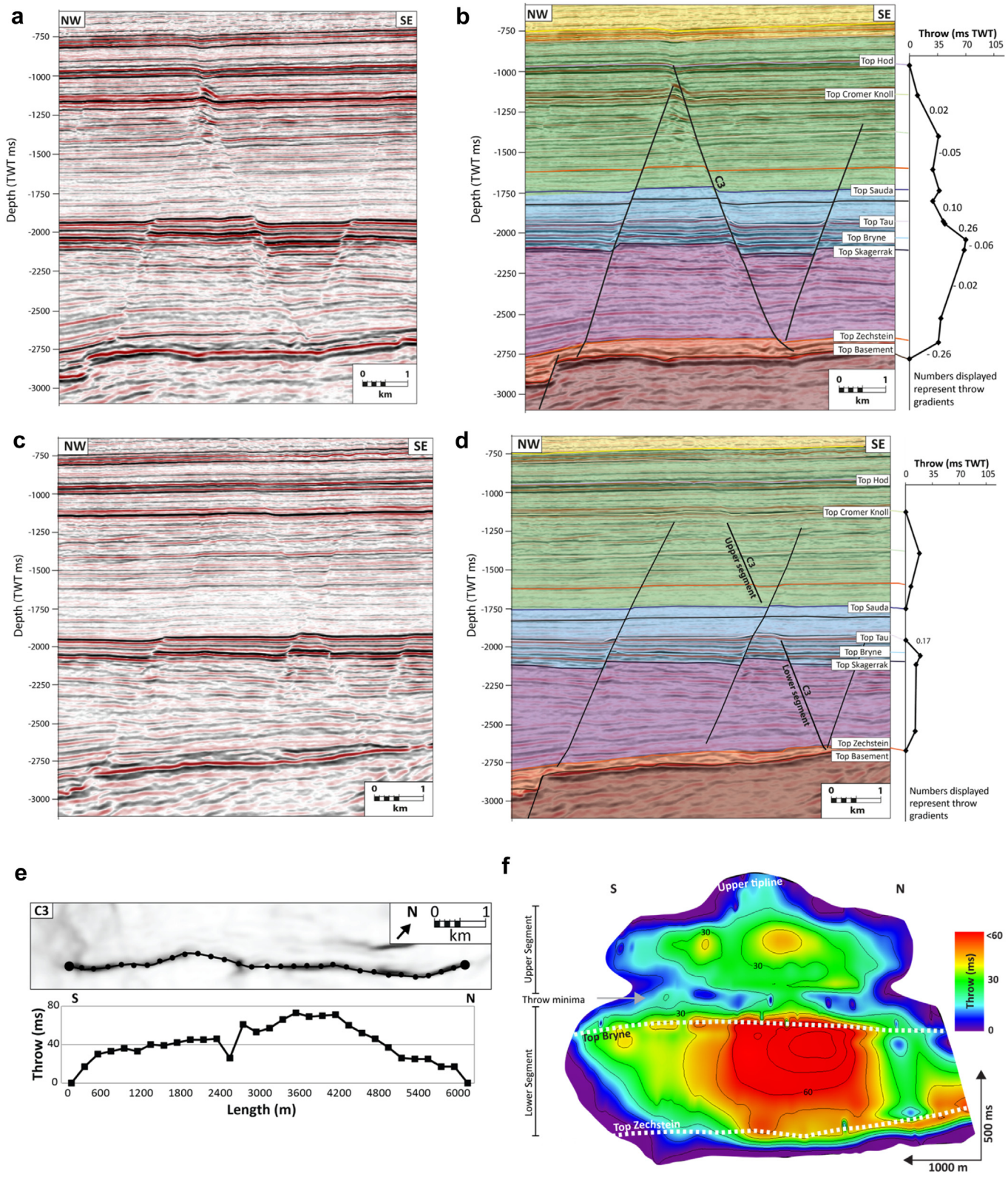

Fig. 10. (a) Seismic profile with cover fault C3 (C3) in the Southern Domain, where (b) is with interpreted horizons and faults. *T-z* plots indicate the asymmetric throw distribution across the location of throw maximum. (c) and (d) Seismic profile illustrating fault C3 north of profile in (a) and (b). Cover Fault C3 has an upper and lower segment as indicated on the *T-z* curve. (e) Variance map of fault C3 with corresponding throw length profile along the top of the Bryne Formation showing gradual decrease in throw toward the northern and southern fault tips. (f) Throw strike-projections on the fault surface illustrating a concentric shape of throw distribution on the upper part of the fault segment, and an asymmetrical shape on the lower part of the fault segment.

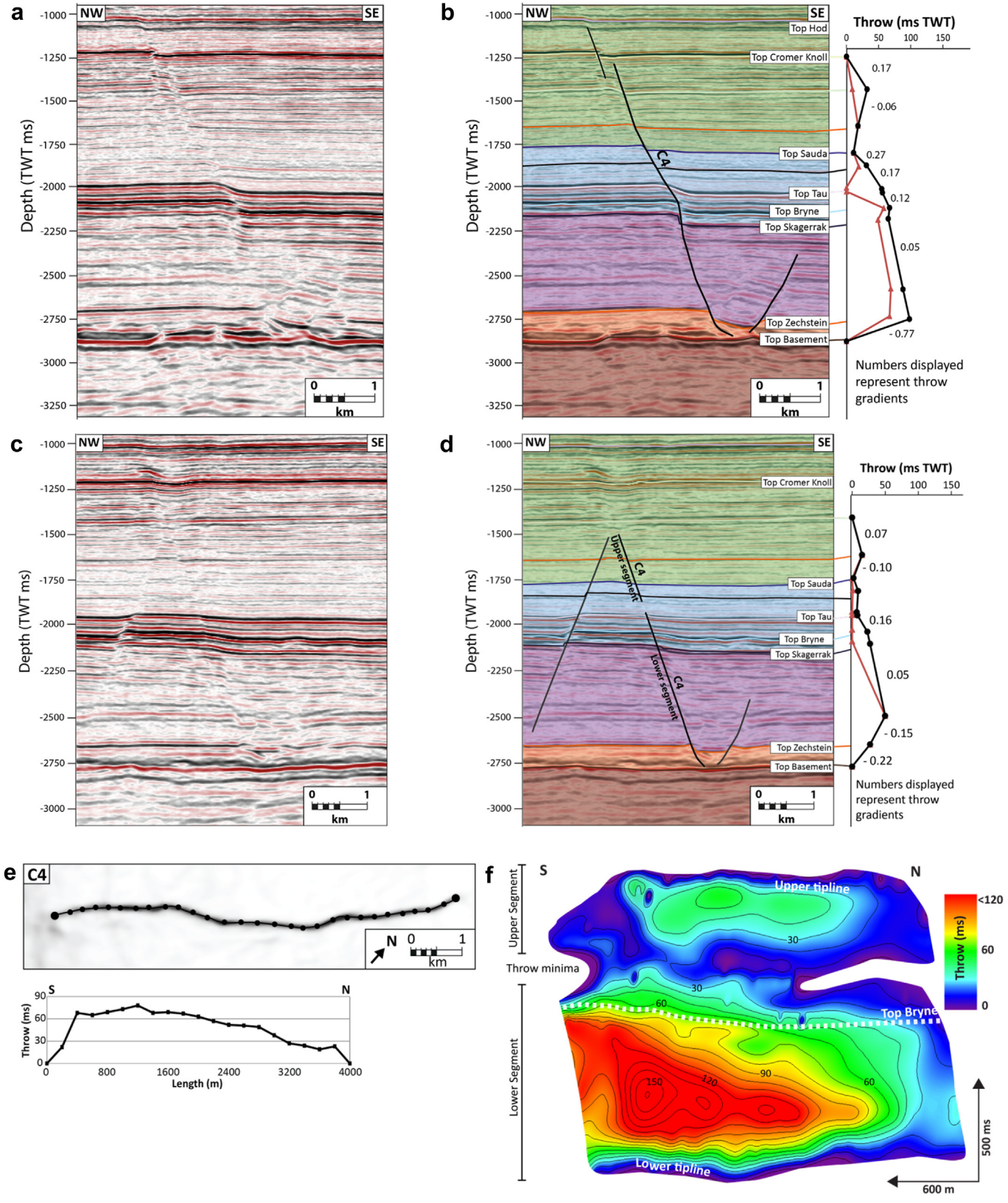

Fig. 11. (a) Seismic profile with cover fault C4 in the Southern Domain, where (b) is with interpreted horizons and faults. (c) and (d) Showing fault segments which split along strike into an upper and lower segment. *T-z* plots perpendicular to strike of the fault plane (red line indicating where drag is not included in the picks, while black line indicates where throw is recorded at inflection points of the drag folds. (e) Variance map of Cover Fault C4 with corresponding throw length profile showing gradual decrease in throw toward the northern fault tip, while more rapid decreasing throw toward the southern fault tip. (f) Throw strike-projections on the fault plane showing the asymmetrical throw distribution. (For interpretation of the references to colour in this figure legend, the reader is referred to the web version of this article.)

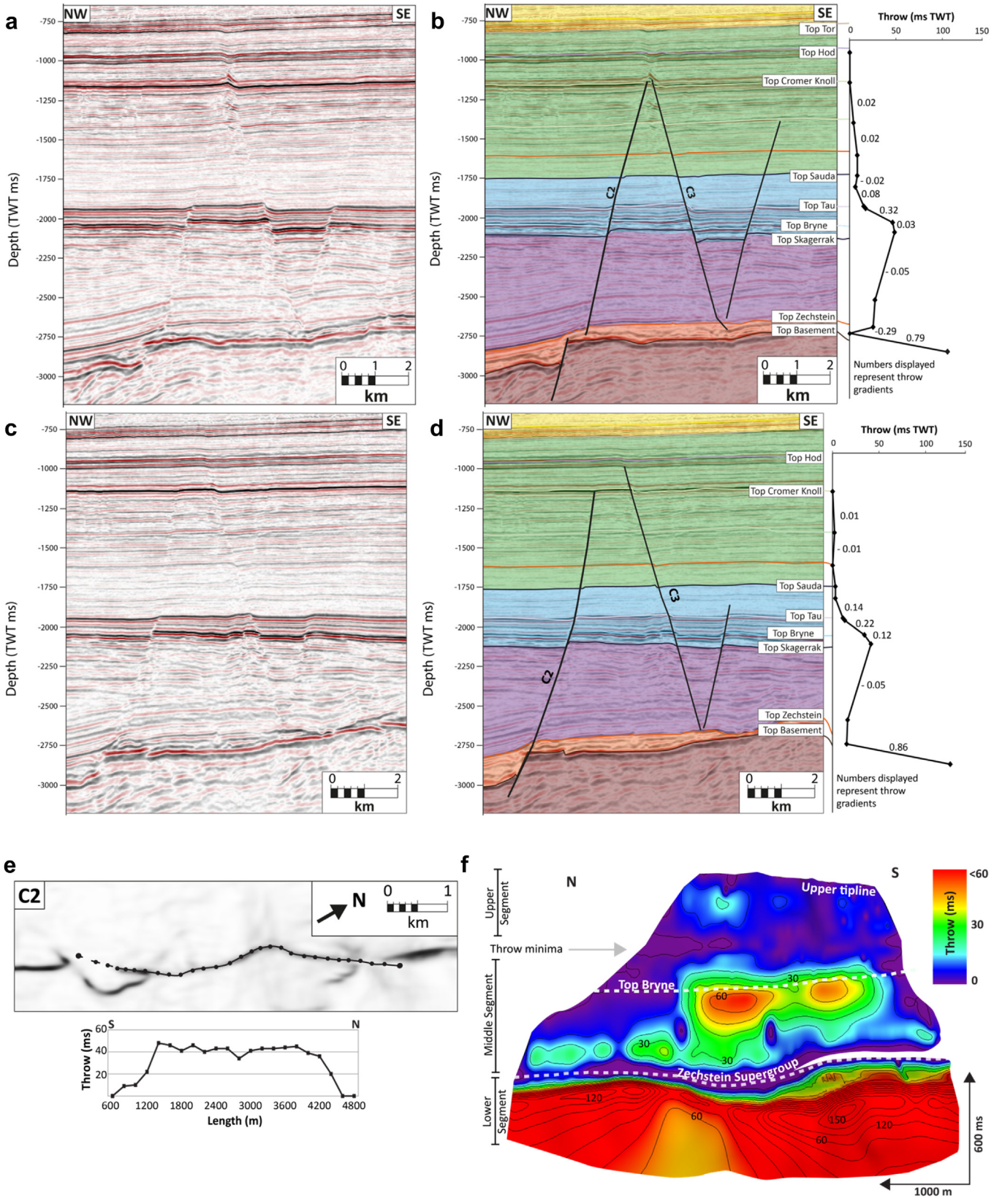

Fig. 12. (a) and (b) Seismic profile perpendicular to strike of the Cover Fault C2 in the Southern Domain. Here the fault offsets the basement, while in figure (c) and (d) a flat-ramp structure decoupling the basement fault from C2,as shown by the *T-z* plots in (b) and (d). (e) Variance map of fault C2 with corresponding throw-length profile along the Top Bryne Formation showing one throw minima at 2900 m, which can be an indication of early linkage of two individual fault segments. This linkage is also indicated on (f) the throw strike-projection on the fault surfaces with two bulls' eyes at level of Top Bryne. Throw strike-projections also illustrate the coupled and decoupled relationship between the lower and middle segment through the salt.

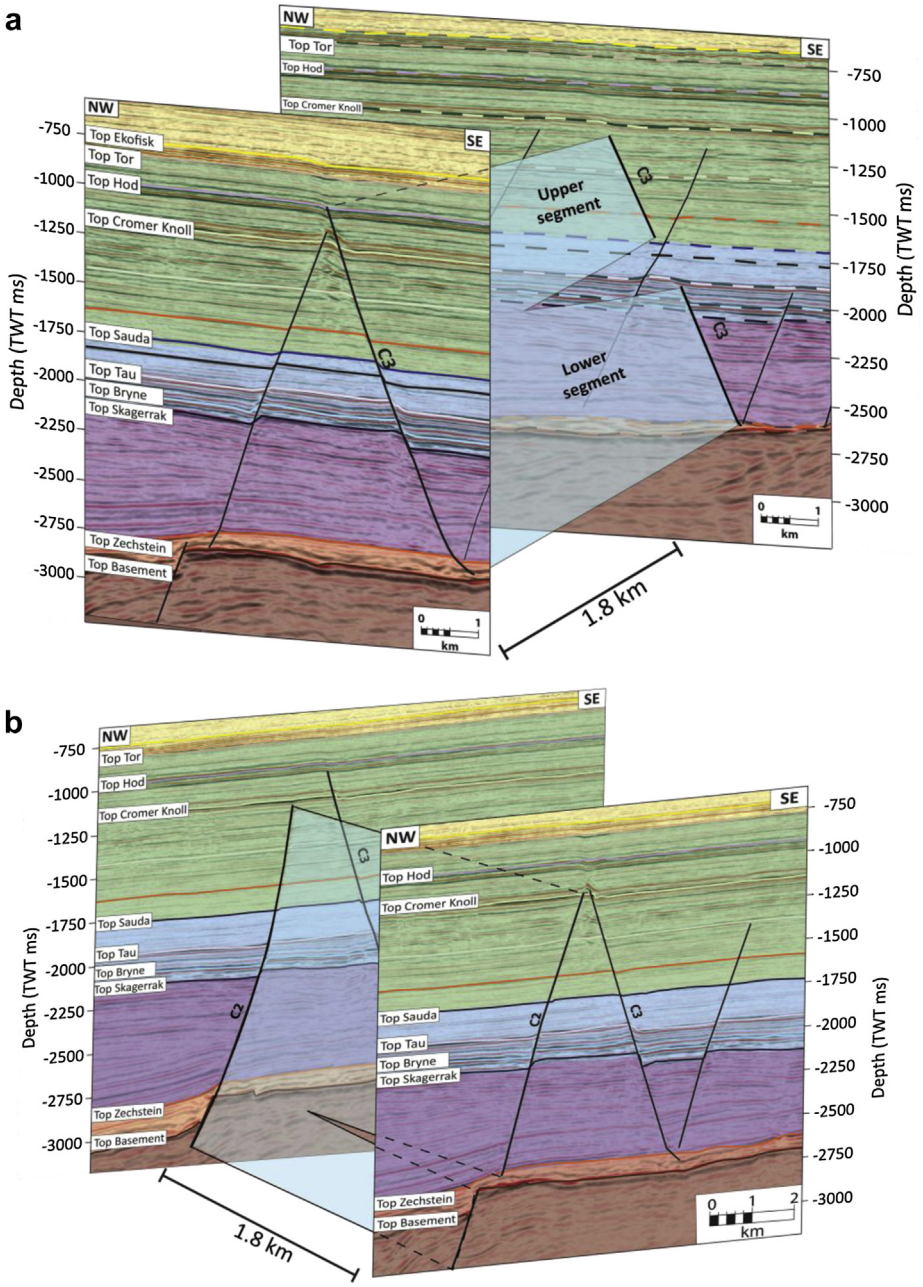

Fig. 13. (a) Illustration of bifurcation of cover fault C3 along strike, where a single fault surface passes along-strike into two, laterally offset segments. (b) Illustration of the interaction between the basement and cover fault C2.

blind propagation of pre-existing, buried faults (i.e. the 'classic' model for fault reactivation; Richard and Krantz, 1991) or 2) by nucleation of a newly formed fault segment in the 'cover', in Lower Cretaceous strata, which propagated downward (and upward) before linking with the deeper segment (Fig. 14) (Baudon and Cartwright, 2008b). We suggest the latter model is applicable for faults in the Southern Domain, based on the observation that two throw maxima are developed. One is below and one above the Jurassic mudstone-dominated detachment, which are separated by a zone of little or no throw (Figs. 14c and d and 15). We interpret that folding adjacent to this style of fault documents upward propagation and fault-related folding ahead of the upward-propagating, lower segment; eventual linkage of the upper and lower segment leads to breaching of the fold and its preservation in the hanging wall of the now-linked structure (Mansfield and Cartwright, 2001; Rykkelid and Fossen, 2002).

6. Trigger for nucleation and growth of the cover-restricted fault array

A key question is "What caused the nucleation and growth of the cover-restricted fault array?" The north-western part of the Egersund Basin is defined by a west-dipping half graben, which is bound by the east-dipping Sele High Fault System. Sub-salt, Lower Permian (and older) strata, and the salt-basement contact, dip westward toward the basin-bounding fault (Fig. 16), implying that the thin-skinned fault array could have simply formed as a gravity-

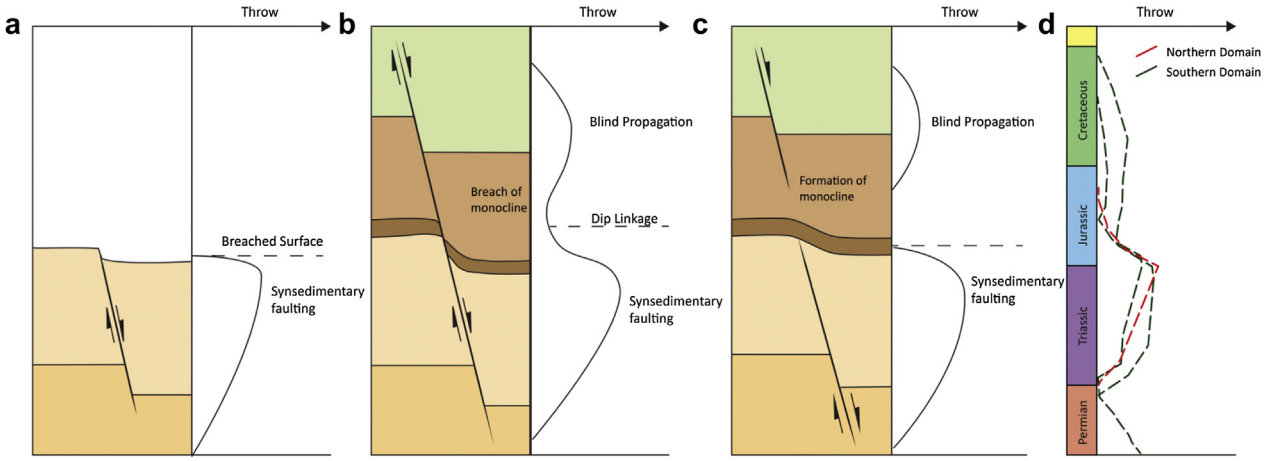

Fig. 14. Simplified illustrations of a vertical throw distribution plots for (a) a syn-sedimentary fault, such as the faults in the northern domain; (b) for a fault which first was syn-sedimentary with a blind fault nucleating in the overburden and propagating to interact with the syn-sedimentary fault; and (c) syn-sedimentary fault with a blind fault nucleating in the overburden. The blind propagation of faults forms a monocline with the shale which acts more ductilly. As the two faults propagate, the monocline is breached resulting in coupled deformation as in (b). (d) Simplified vertical-throw profiles from this study for comparison.

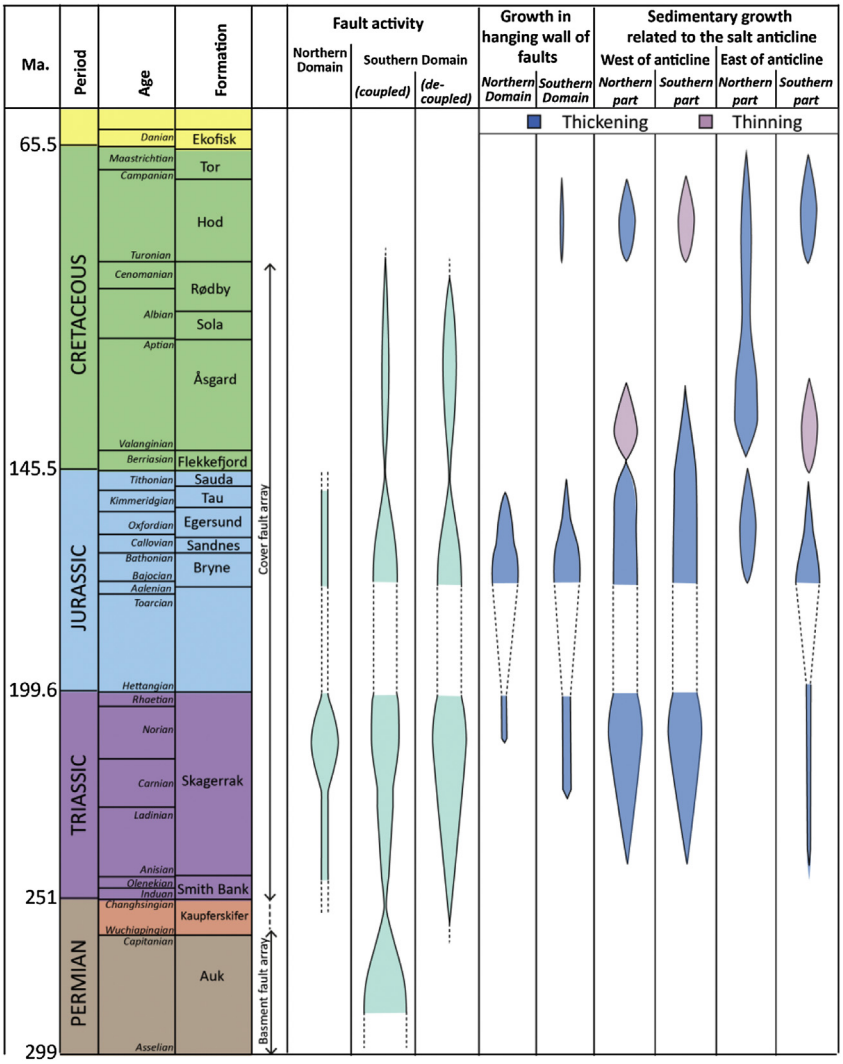

Fig. 15. Summary of analyses for this study. Fault activity is illustrated by wider shaded area for greater throw. Hanging wall growth of faults illustrating the thickening of different formations in the hanging wall, and sedimentary growth on either side of the salt anticline are based on the thickness maps and expansion indices (see Figs. 8, 9 and 17).

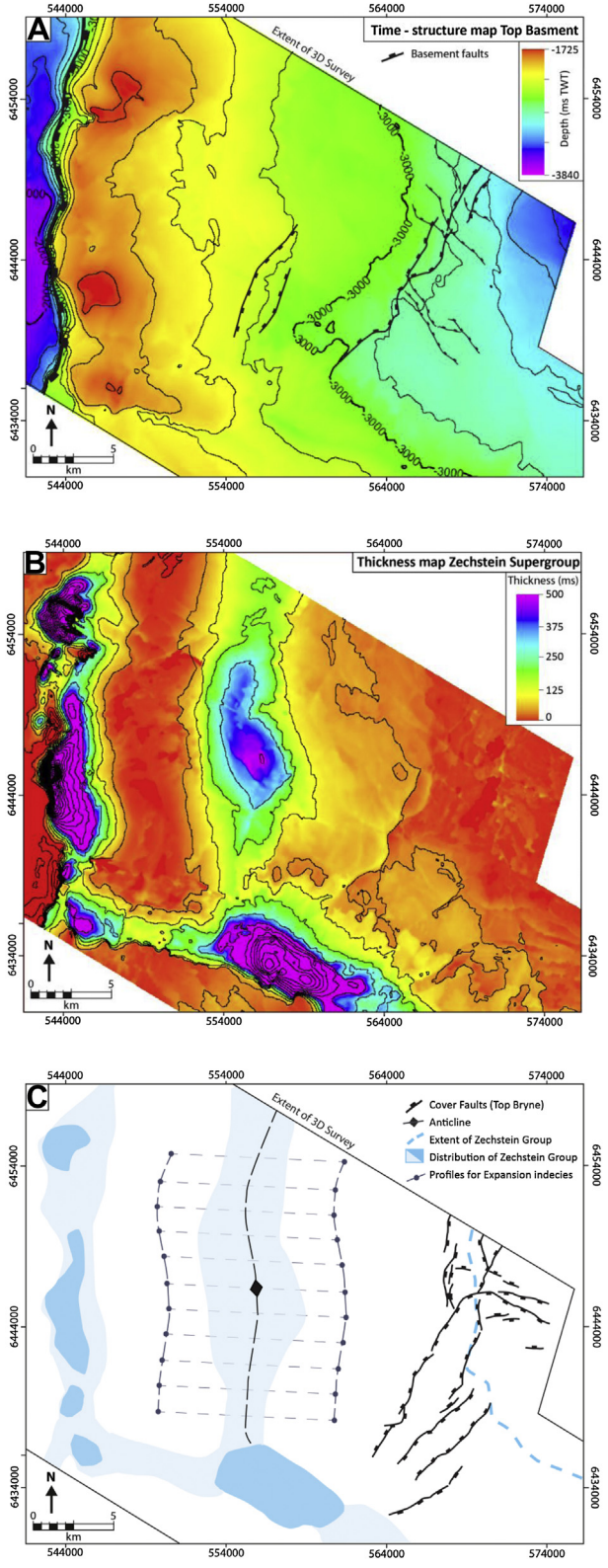

Fig. 16. (a) Time structure map of Top Basement with basement fault array on top and the Sele High Fault System to the west. (b) Isochron thickness map of the ZSG. (c) The salt anticline is close to parallel to the salt wall with diapirs to the west and the studied fault array in the east. The lines on either side of the salt anticline represent profiles used for expansion indices in Fig. 17.

driven system, triggered by basin margin faulting and associated basement tilting. This interpretation would be consistent with the mean NNE–SSW trend of the thin-skinned fault array. However, salt mobilization, in the absence of thick-skinned tectonics, can also occur. To assess whether the studied fault array formed in response to thick-skinned extension and 'passive' gravity-gliding above the salt or active growth of a salt structure, which may or may not have been linked to basement-involved tectonics, we need to assess the pattern of the salt mobilization.

6.1. Timing of salt mobilization

Several salt structures are developed in the north-western part of the Egersund Basin. One of these structures is a broadly ENE–WSW-trending salt anticline. This anticline displays relief of 500 ms (1019 m) and it is flanked to the west by an apparent weld, where the salt would be very thin or absent (Figs. 2, 9e and 16b) (Wagner III and Jackson, 2011). Because it is located only 10 km to the west of, and has the same strike length as and trends sub-parallel to the fault array, we speculate that salt flow related to the growth of this anticline was responsible for the nucleation and growth of cover-restricted fault array (Figs. 5 and 16b and c). We therefore use seismic-stratigraphic observations from seismic profiles, supra-salt isochron maps and isochron thinning ratios (*sensu* Higgins et al., 2009; see also Jackson et al., 2013) to assess the timing of formation of this salt anticline, and its temporal relationship to the cover-restricted fault array (Figs. 9, 16 and 17). Isochron thinning ratios illustrate the ratio between the sediment thickness above the salt anticline and the thickness of the same unit 6 km to the west and east of the salt anticline. The profile to the west of the anticline is located above the salt weld and the one to the east is located between the anticline and the fault array (Figs. 16b–c and 17).

Our analysis indicates that the Lower Triassic interval is broadly tabular and concordant with the folded upper surface of the salt anticline, whereas the upper part of the Skagerrak Formation (Carnian-to-Rhaetian age strata), the Bryne, Egersund, Sandnes and Tau Formations, and the lower part of Sauda Formation (i.e. middle Aalenian–to-middle Tithonian age strata) thin across the salt anticline (Figs. 9e and 17). Major thickening of the Carnian-to-Rhaetian interval of the Skagerrak Formation is only observed down the western flank of the anticline, implying that the structure was primarily growing in response to salt withdrawal from the west, below the subsiding minibasin in the region of the future weld (Fig. 17a). It is important to note that some thinning may have been caused by erosion along the Intra Aalenian Unconformity (Husmo et al., 2003), but from seismic profiles and growth analysis it is clear that some of the thickening is related to true syn-sedimentary structural growth (Fig. 9e). From the Bajocian to the Bathonian, further growth of the anticline is demonstrated by thickness variations in the Bryne Formation. However, in contrast to the Triassic times, stratal thickening is asymmetric along strike of the western limb, and most pronounced along the southern end of the structure, implying preferential growth of the salt anticline in this location at this time. Furthermore, thinning of Bajocian-to-Bathonian strata onto the eastern flank of the anticline is observed at this time, implying that: (i) salt was now being withdrawn from east of the anticline; or (ii) that structures along the newly initiated, cover-restricted fault array were responsible for generating accommodation and thicker successions to the east of the anticline. After a period of relatively dramatic growth in the Triassic and Middle Jurassic (i.e. expansion indices of up to 4.5), growth of the salt anticline during the Late Jurassic and Cretaceous appears to have been more moderate (i.e. expansion indices <1.5). Almost no growth occurred in the Albian to Cenomanian, before a

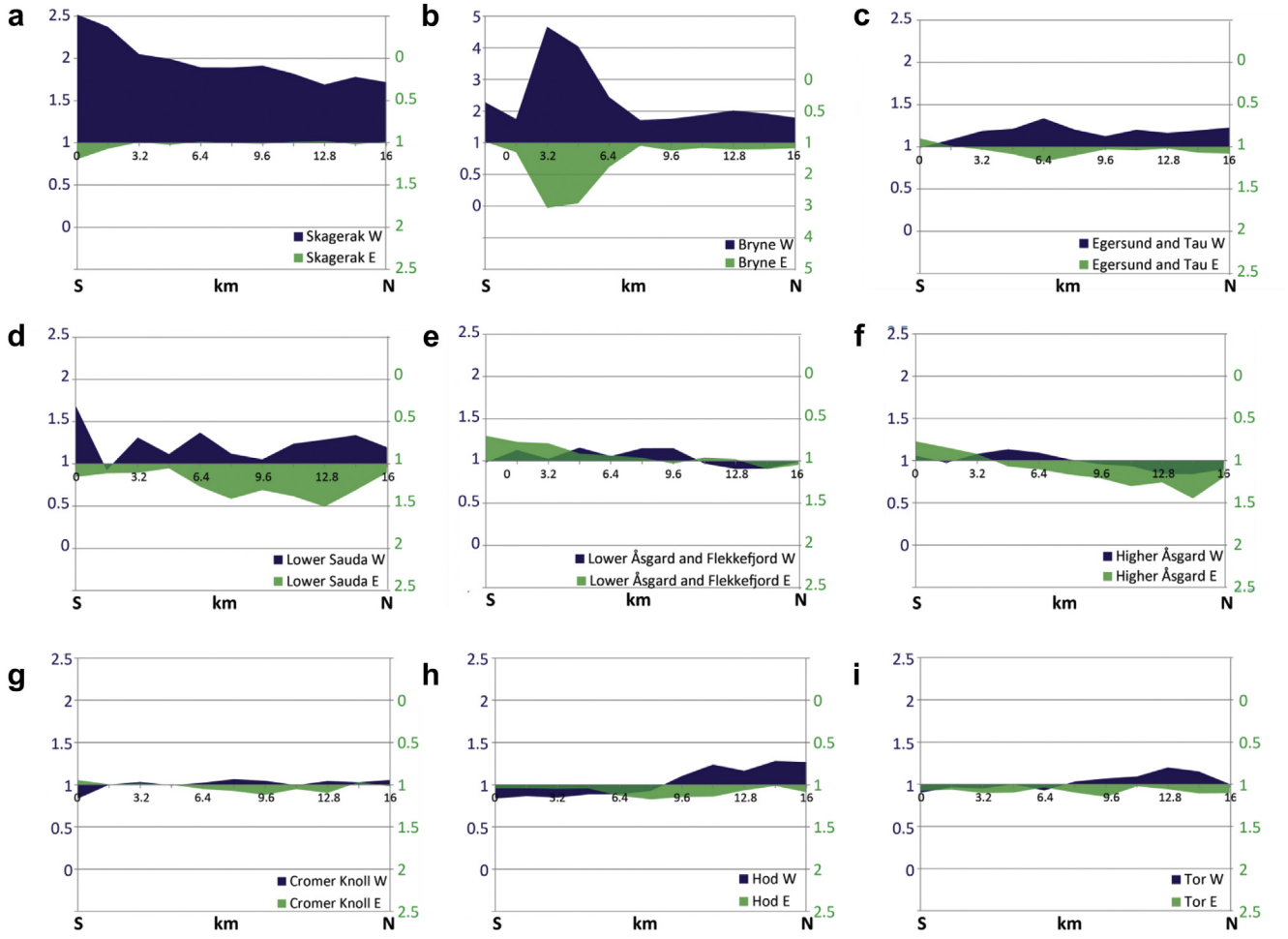

Fig. 17. Profiles of expansion indices for the sedimentary formations on the western (Dark purple) and eastern side (green) of the salt anticline (for profile locations see Fig. 16c); (a) The upper part of the Skagerrak Formation; (b) the Egersund Formation (note the change in axis values on this specific profile); (c) the Egersund and Tau Formations; (d) the Sauda Formation; (e) the Lower part of Åsgard and the Flekkefjord Formation; (f) the higher part of the Åsgard Formation; (g) the Cromer Knoll Group; (h) the Hod Formation; and (i) the Tor Formation. The axes to the left give the expansion index value for the western side of the salt anticline, while the ones to the right are for the eastern side of the salt anticline. Note that the axis values are the same on every figure with the exception of (b). (For interpretation of the references to colour in this figure legend, the reader is referred to the web version of this article.)

second period of anticline growth occurred during the Turonian to Campanian, which was principally associated with growth in the north while thinning in the south on the western side of the salt anticline (Figs. 9d and 17h). The same pattern can also be recognized in strata of Maastrichtian age (i.e. Tod Formation), along the smaller thickness variations imply slower rates of growth (Fig. 17i).

6.2. Controls on salt mobilization

These analyses indicate that salt flow and growth of the anticline was pulsed, and can be divided into two stages. The first stage occurred in the Late Triassic (Carnian times) (Hospers et al., 1988; Sørensen et al., 1992; Goldsmith et al., 2003). Hospers et al. (1988) claimed that a large amount of salt structures developed independent of faulting and were randomly distributed in the flat-bottomed, deep part of the Norwegian–Danish Basin. In contrast, Koyi and Petersen (1993) argued that the salt structures were largely controlled by basement faults. We suggest that in the Triassic, activity on the Sele High Fault System caused basement tilting and salt flow, possibly due to the withdrawal of salt from the western side of the anticline to feed a salt wall that developed in the immediate hanging wall of the Sele High Fault System (Fig. 18a–c). The second stage of salt mobilization occurred during the Late Cretaceous (Figs. 9d, 17h–i and 18e–f), possibly in response to basin shortening and inversion (Jackson et al., 2013). Diapir rejuvenation and 'active' diapirism has also been suggested for the large salt diapirs in Central Graben, North Sea (Davison et al., 2000).

7. Discussion

7.1. What triggered nucleation and growth of the cover-restricted fault array?

A clear spatial relationship exists between the cover- and basement-restricted fault arrays. Previous studies have shown that cover-restricted fault arrays are more likely to develop nearby and strike sub-parallel to, basement-restricted faults, because flexure, tilting and gravity gliding of the cover above basement faults can lead to fault nucleation and growth (Vendeville et al., 1995; Erratt et al., 1999; Withjack and Callaway, 2000). We propose that Triassic activity on the Sele High Fault System triggered westward gliding and mobilization of salt, and formation of the cover-restricted fault array due to thin-skinned extension of the Triassic cover (Fig. 18a–d). Based on the spatial relationship between the cover- and basement-restricted fault arrays, we propose that flexure of the cover across a series of sub-salt steps associated with

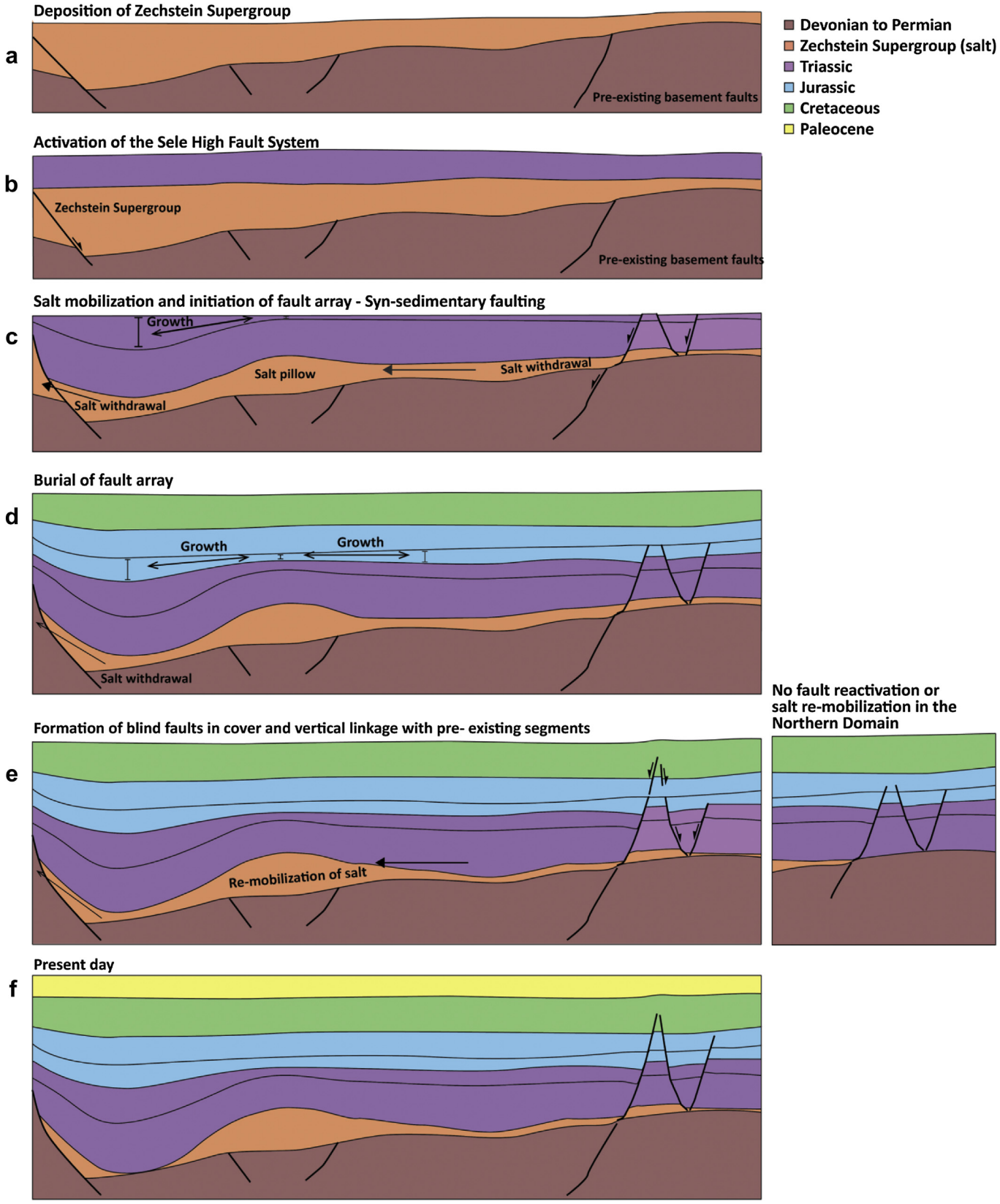

Fig. 18. Simplified sketch of the evolution of the fault array. (a) to (c) Late Triassic cover faults developed from pre-existing basement-bounding faults and contemporaneous salt mobilization during the Middle to late Triassic. This resulted in formation of the cover fault array in the Late Triassic. (d) The faulting continued into the Upper Jurassic when the tectonic activity ceased and the cover fault array was buried. (e) Late Cretaceous inversion triggered re-mobilization of salt which led to nucleation of blind faults in the cover, which again reactivated some faults within the fault array (f). To the North where the Zechstein Group was already depleted by the Middle Jurassic, no reactivation occurred (e).

basement-restricted faults controlled the initiation and localisation of the cover-restricted fault array. The Sele High Fault System acted as a downdip buttress, which resulted in the formation of a salt-cored buckle fold that was principally fed by salt derived from its western margin. Death of the fault array probably occurred in response to the development of the salt weld, and the cessation of salt flow and cover gravity gliding.

We speculate that mild reactivation of the cover-restricted fault array in the Southern Domain was triggered by Late Cretaceous (Turonian) basin inversion (Jackson et al., 2013), which cause shortening and amplification of the salt anticline, which may have resulted in local extension of the cover updip to the east. The location of basement-restricted faults and salt thickness controlled the location and style of cover-restricted fault growth at this time. For example, in the northern part of the fault array, where the salt is relatively thin, the cover-restricted faults were *not* reactivated (Fig. 18e). In the southern part of the fault array, where the salt is relatively thick, cover faults *were* reactivated, and new faults formed in the Cretaceous overburden (Fig. 18e and f). Furthermore, salt thickness has a clear relationship to the magnitude of lateral offset between basement and cover faults; i.e. cover faults in the north are co-linear in cross-section with basement faults, whereas in the south, lateral offset between these two fault populations scales roughly with the thickness of the salt. These observations are in general agreement with the predictions of scaled physical models by Withjack and Callaway (2000), who indicated a close relationship between the style and distribution of supra-salt deformation and the thickness of salt, where the lateral offset between basement faults and cover faults increases with increasing salt thickness.

7.2. Growth of normal faults in mechanically layered sequences

The growth of the fault array was influenced by mechanically layered nature of the host rock. For example, salt locally controlled the degree and style of coupling between sub- and supra-salt deformation, and thick mudstone-dominated units in the cover controlled the growth and final structural style of several structures in the cover-restricted fault systems. The fact that through-going, basement-involved faults bifurcate and pass along strike into physically separate, laterally distinct segments, which are decoupled by salt, implies that in the latter location, the segments are *kinematically coupled* despite being *geometrically decoupled*. This relationship suggests that kinematic coherency between sub- and supra-salt segments is maintained by sub-seismic, distributed, ductile strains within the salt (Childs et al., 1996; Schöpfer et al., 2006). A similar interpretation can be applied to the relationship between cover-restricted faults that bifurcate along strike. In this case, thick mudstones, rather than salt, deform by ductile flow and serve to maintain kinematic coherency between the sub- and supra-mudstone segments. This model of segmented fault growth by fault formation in 'strong', brittle layers and, at least at low strains, ductile flow in 'weak' layers is consistent with the results of discrete element models (DEM) of Schöpfer et al. (2006).

8. Conclusions

This study has provided a detailed analysis of the geometry and throw distribution of a thin-skinned fault array located immediately south–east of a low-relief salt anticline. We conclude that the supra-salt fault array evolved in stages of (i) syn-depositional growth faulting at the free surface due to salt mobilization triggered by Triassic extension along major basin-bounding basement faults; (ii) tectonic quiescence and burial of the fault tips Upper Jurassic to Turonian times; and (iii) salt re-mobilization triggered by basin inversion initiated in the Turonian, leading to blind reactivation in parts of the fault array (Figs. 15 and 18).

The driving mechanism behind fault activation and reactivation, and thus the overall evolution of the fault array is a combination between basement faulting and salt (re-)mobilization in response to regional tectonic events. In the final part of the evolution of the fault array, reactivation appears to have been largely controlled by salt mobilization in response to basin inversion without reactivation of the *basement-involved fault array*, because faults that show blind reactivation at this stage are located where the underlying salt is thick, while the non-reactivated faults are found where salt is near depleted. Hence, reactivation only occurred where salt mobilization was able to affect the fault array. The fault array provides an example of sub- and supra-salt faults that are geometrically un-linked through the salt along most of its extent, but locally physically linked where strains were sufficiently large to discretely breach the ZSG. However, despite the large extent of geometric decoupling across the ZSG, deformation was kinematically coupled, in the sense that the basement faults still affected the nucleation and localization of the cover faults.

Acknowledgements

We thank Brent Couzens-Schultz, an anonymous reviewer and Editor William M. Dunne for their thorough reviews, which greatly improved this article. We also thank PGS for access to seismic data and also granting permission to publish. In particular, we thank Richard Lamb at PGS for his assistance in securing relevant permissions to access and publish images from these data. We also thank Schlumberger for providing access to Petrel software and Badleys Geosciences for their TrapTester modelling software.

References

Baudon, C., Cartwright, J., 2008a. Early stage evolution of growth faults: 3D seismic insights from the Levant Basin, Eastern Mediterranean. Journal of Structural Geology 30, 888–898.

Baudon, C., Cartwright, J., 2008b. The kinematics of reactivation of normal faults using high resolution throw mapping. Journal of Structural Geology 30, 1072–1084.

Brown, A.R., 2003. Interpretation of Three-dimensional Seismic Data, sixth ed., vol. 42. American Association of Petroleum Geologists Memoir, p. 541.

Childs, C., Nicol, A., Walsh, J.J., Watterson, J., 1996. Growth of vertically segmented normal faults. Journal of Structural Geology 18, 1389–1397.

Childs, C., Nicol, A., Walsh, J.J., Watterson, J., 2003. The growth and propagation of synsedimentary faults. Journal of Structural Geology 25, 633–648.

Childs, C., Watterson, J., Walsh, J.J., 1995. Fault overlap zones within developing normal fault systems. Journal of the Geological Society 152, 535–549.

Davison, I., Alsop, I., Birch, P., Elders, C., Evans, N., Nicholson, H., Rorison, P., Wade, D., Woodward, J., Young, M., 2000. Geometry and late-stage structural evolution of Central Graben salt diapirs, North Sea. Marine and Petroleum Geology 17, 499–522.

Duffy, O.B., Gawthorpe, R.L., Docherty, M., Brocklehurst, S.H., 2012. Mobile evaporite controls on the structural style and evolution of rift basins: Danish Central Graben, North Sea. Basin Research 25, 310–330.

Erratt, D., Thomas, G.M., Wall, G.R.T., 1999. The evolution of the Central north sea rift. In: Geological Society, London, Petroleum Geology Conference Series, vol. 5, pp. 63–82.

Ford, M., Le Carlier de Veslud, C., Bourgeois, O., 2007. Kinematic and geometric analysis of fault-related folds in a rift setting: the Dannemarie basin, Upper Rhine Graben, France. Journal of Structural Geology 29, 1811–1830.

Gawthorpe, R.L., Leeder, M.R., 2000. Tectono-sedimentary evolution of active extensional basins. Basin Research 12, 195–218.

Glennie, K.W., Higham, J., Stemmerik, L., 2003. Permian. In: Evans, D., Graham, C., Armour, A., Bathurst, P. (Eds.), The Millennium Atlas: Petroleum Geology of the Central and Northern North Sea. The Geological Society of London, London.

Goldsmith, P., Hudson, G., Van Veen, P., 2003. Triassic. In: Evans, D., Graham, C., Armour, A., Bathurst, P. (Eds.), The Millennium Atlas: Petroleum Geology of the Central and Northern North Sea. The Geological Society of London, London.

Higgins, S., Clarke, B., Davies, R.J., Cartwright, J., 2009. Internal geometry and growth history of a thrust-related anticline in a deep water fold belt. Journal of Structural Geology 31, 1597–1611.

Hodgson, N.A., Farnsworth, J., Fraser, A.J., 1992. Salt-related tectonics, sedimentation and hydrocarbon plays in the Central Graben, North Sea, UKCS. In: Geological Society, London, Special Publications, vol. 67, pp. 31–63.
Hongxing, G., Anderson, J.K., 2007. Fault throw profile and kinematics of normal fault-conceptual models and geologic examples. Geological Journal of China Universities 13, 75–88.
Hospers, J., Rathore, J.S., Jianhua, F., Finnstrøm, E.G., Holthe, J., 1988. Salt tectonics in the Norwegian–Danish basin. Tectonophysics 149, 35–60.
Husmo, T., Hamar, G., Høiland, O., Johannessen, E.P., Rømuld, A., Spencer, A., Titterton, R., 2003. Lower and middle Jurassic. In: Evans, D., Graham, C., Armour, A., Bathurst, P. (Eds.), The Millennium Atlas: Petroleum Geology of the Central and Northern North Sea. The Geological Society of London, London.
Isaksen, D., Tonstad, K., 1989. A Revised Cretaceous and Tertiary Lithostratigraphic Nomenclature for the Norwegian North Sea. Oljedirektoratet, Stavanger.
Jackson, C.-L., Chua, S.-T., Bell, R., Magee, C., 2013. Structural style and early stage growth of inversion structures: 3D seismic insights from the Egersund Basin, offshore Norway. Journal of Structural Geology 46, 167–185.
Jackson, C.A.L., Rotevatn, A., 2013. 3D seismic analysis of the structure and evolution of a salt-influenced normal fault zone: a test of competing fault growth models. Journal of Structural Geology. ISSN:0191-8141.
Jackson, C.A.L., Lewis, M.M., 2012. Origin of an anhydrite sheath encircling a salt diapir and implications for the seismic imaging of steep-sided salt structures, Egersund Basin, Northern North Sea. Journal of the Geological Society 169, 593–599.
Jackson, M.P.A., Hudec, M.R., 2005. Stratigraphic record of translation down ramps in a passive-margin salt detachment. Journal of Structural Geology 27, 889–911.
Jackson, M.P.A., Vendeville, B.C., 1994. Regional extension as a geologic trigger for diapirism. Geological Society of America Bulletin 106, 57–73.
Kane, K.E., Jackson, C.A.L., Larsen, E., 2010. Normal fault growth and fault-related folding in a salt-influenced rift basin: south Viking Graben, offshore Norway. Journal of Structural Geology 32, 490–506.
Koyi, H., Petersen, K., 1993. Influence of basement faults on the development of salt structures in the Danish Basin. Marine and Petroleum Geology 10, 82–94.
Mansfield, C., Cartwright, J., 2001. Fault growth by linkage: observations and implications from analogue models. Journal of Structural Geology 23, 745–763.
Mansfield, C.S., Cartwright, J.A., 1996. High resolution fault displacement mapping from three-dimensional seismic data: evidence for dip linkage during fault growth. Journal of Structural Geology 18, 249–263.
Marsh, N., Imber, J., Holdsworth, R.E., Brockbank, P., Ringrose, P., 2010. The structural evolution of the Halten Terrace, offshore Mid-Norway: extensional fault growth and strain localisation in a multi-layer brittle-ductile system. Basin Research 22, 195–214.
Maurin, J.-C., Niviere, B., 2000. Extentional forced folding and decollement of the pre-rift series along the Rhine graben and their influence on the geometry of the syn-rift sequences. In: Special Publication – Geological Society of London, vol. 169, pp. 73–86.
Morley, C., Back, S., Van Rensbergen, P., Crevello, P., Lambiase, J., 2003. Characteristics of repeated, detached, Miocene–Pliocene tectonic inversion events, in a large delta province on an active margin, Brunei Darussalam, Borneo. Journal of Structural Geology 25, 1147–1169.
Møller, J.J., Rasmussen, E.S., 2003. Middle Jurassic–Early Cretaceous rifting of the Danish Central graben. Geological Survey of Denmark and Greenland Bulletin 1, 247–264.
Nicol, A., Watterson, J., Walsh, J.J., Childs, C., 1996. The shapes, major axis orientations and displacement patterns of fault surfaces. Journal of Structural Geology 18, 235–248.
Pascoe, R., Hooper, R., Storhaug, K., Harper, H., 1999. Evolution of extensional styles at the southern termination of the Nordland Ridge, Mid-Norway: a response to variations in coupling above Triassic salt. In: Geological Society, London, Petroleum Geology Conference Series. Geological Society of London.
Richard, P., Krantz, R.W., 1991. Experiments on fault reactivation in strike-slip mode. Tectonophysics 188, 117–131.
Richardson, N.J., Underhill, J.R., Lewis, G., 2005. The role of evaporite mobility in modifying subsidence patterns during normal fault growth and linkage, Halten Terrace, Mid-Norway. Basin Research 17, 203–223.
Rouby, D., Guillocheau, F., Robin, C., Bouroullec, R., Raillard, S., Castelltort, S., Nalpas, T., 2003. Rates of deformation of an extensional growth fault/raft system (offshore Congo, West African margin) from combined accommodation measurements and 3-D restoration. Basin Research 15, 183–200.
Rowan, M.G., Jackson, M.P.A., Trudgill, B.D., 1999. Salt-related fault families and fault welds in the northern Gulf of Mexico. Aapg Bulletin 83, 1454–1484.
Rykkelid, E., Fossen, H., 2002. Layer rotation around vertical fault overlap zones: observations from seismic data, field examples, and physical experiments. Marine and Petroleum Geology 19, 181–192.
Schöpfer, M.P., Childs, C., Walsh, J.J., 2006. Localisation of normal faults in multilayer sequences. Journal of Structural Geology 28, 816–833.
Stewart, S.A., Ruffell, A.H., Harvey, M.J., 1997. Relationship between basement-linked and gravity-driven fault systems in the UKCS salt basins. Marine and Petroleum Geology 14, 581–604.
Sørensen, S., Morizot, H., Skottheim, S., 1992. A tectonostratigraphic analysis of the Southeast Norwegian North Sea basin. In: Special Publication – Norwegian Petroleum Society, NPF, vol. 1, pp. 19–42.
Thorsen, C.E., 1963. Age of growth faulting in southeast Louisiana. Gulf Coast Association of Geological Societies 13, 103–110.
Underhill, J.R., Partington, M.A., 1993. Jurassic thermal doming and deflation in the North Sea: implications of the sequence stratigraphic evidence. In: Geological Society, London, Petroleum Geology Conference Series, vol. 4, pp. 337–345.
Van Rensbergen, P., Morley, C., Ang, D., Hoan, T., Lam, N., 1999. Structural evolution of shale diapirs from reactive rise to mud volcanism: 3D seismic data from the Baram delta, offshore Brunei Darussalam. Journal of the Geological Society 156, 633–650.
Vejbæk, O., Andersen, C., 2002. Post mid-Cretaceous inversion tectonics in the Danish Central Graben—regionally synchronous tectonic events. Bulletin of the Geological Society of Denmark 49, 129–144.
Vendeville, B., Ge, H., Jackson, M., 1995. Scale models of salt tectonics during basement-involved extension. Petroleum Geoscience 1, 179–183.
Vendeville, B.C., Jackson, M.P.A., 1992. The fall of diapirs during thin-skinned extension. Marine and Petroleum Geology 9, 354–371.
Vollset, J., Doré, A.G., 1984. A Revised Triassic and Jurassic Lithostratigraphic Nomenclature for the Norwegian North Sea. Oljedirektoratet, Stavanger.
Wagner III, B.H., Jackson, M., 2011. Viscous flow during salt welding. Tectonophysics 510, 309–326.
Walsh, J.J., Watterson, J., 1988. Analysis of the relationship between displacements and dimensions of faults. Journal of Structural Geology 10, 239–247.
Walsh, J.J., Watterson, J., 1990. New methods of fault projection for coalmine planning. Proceedings of the Yorkshire Geological and Polytechnic Society 48, 209–219.
Walsh, J.J., Watterson, J., 1991. Geometric and kinematic coherence and scale effects in normal fault systems. In: Geological Society, London, Special Publications, vol. 56, pp. 193–203.
Watterson, J., 1986. Fault dimensions, displacements and growth. Pure and Applied Geophysics 124, 365–373.
Williams, G., Powell, C., Cooper, M., 1989. Geometry and kinematics of inversion tectonics. In: Geological Society, London, Special Publications, vol. 44, pp. 3–15.
Withjack, M.O., Callaway, S., 2000. Active normal faulting beneath a salt layer: an experimental study of deformation patterns in the cover sequence. Aapg Bulletin 84, 627–651.
Withjack, M.O., Olson, J., Peterson, E., 1990. Experimental models of extensional forced folds (1). Aapg Bulletin 74, 1038–1054.
Zanella, E., Coward, M., 2003. Structural framework. In: Evans, D., Graham, C., Armour, A., Bathurst, P. (Eds.), The Millennium Atlas: Petroleum Geology of the Central and Northern North Sea. The Geological Society of London, London.
Ziegler, P.A., 1992. North Sea rift system. Tectonophysics 208, 55–75.